fractal and fractional

MDPI

Article

Fuzzy Fractional Order PID Tuned via PSO for a Pneumatic Actuator with Ball Beam (PABB) System

Mohamed Naji Muftah [1,2,*], Ahmad Athif Mohd Faudzi [1,3,*], Shafishuhaza Sahlan [1,3] and Shahrol Mohamaddan [4]

[1] Faculty of Electrical Engineering, Universiti Teknologi Malaysia, Skudai 81310, Malaysia
[2] Department of Control Engineering, College of Electronics Technology, Bani Walid P.O. Box 38645, Libya
[3] Centre for Artificial Intelligence and Robotics (CAIRO), Universiti Teknologi Malaysia, Kuala Lumpur 51400, Malaysia
[4] College of Systems Engineering and Science, Shibaura Institute of Technology, Saitama 337-8570, Japan
* Correspondence: namohamed@graduate.utm.my (M.N.M.); athif@utm.my (A.A.M.F.)

Abstract: This study aims to improve the performance of a pneumatic positioning system by designing a control system based on Fuzzy Fractional Order Proportional Integral Derivative (Fuzzy FOPID) controllers. The pneumatic system's mathematical model was obtained using a system identification approach, and the Fuzzy FOPID controller was optimized using a PSO algorithm to achieve a balance between performance and robustness. The control system's performance was compared to that of a Fuzzy PID controller through real-time experimental results, which showed that the former provided better rapidity, stability, and precision. The proposed control system was applied to a pneumatically actuated ball and beam (PABB) system, where a Fuzzy FOPID controller was used for the inner loop and another Fuzzy FOPID controller was used for the outer loop. The results demonstrated that the intelligent pneumatic actuator, when coupled with a Fuzzy FOPID controller, can accurately and robustly control the positioning of the ball and beam system.

Keywords: IPA system; system identification technique; Fuzzy FOPID controller; PSO algorithm; PABB system

Citation: Muftah, M.N.; Faudzi, A.A.M.; Sahlan, S.; Mohamaddan, S. Fuzzy Fractional Order PID Tuned via PSO for a Pneumatic Actuator with Ball Beam (PABB) System. *Fractal Fract.* **2023**, *7*, 416. https://doi.org/10.3390/fractalfract7060416

Academic Editor: António Lopes

Received: 31 March 2023
Revised: 19 May 2023
Accepted: 20 May 2023
Published: 23 May 2023

1. Introduction

The pneumatic system is a commonly used actuator in industrial automation, offering benefits such as affordability, natural cooling, environmental safety, and simplicity [1,2]. These systems have a broad range of applications, from simple processes to complex ones, such as those found in production lines, aeronautics, and the automotive industry [3,4]. Their popularity is due to their durability, ease of maintenance, and safety [5]. However, pneumatic systems have a significant downside, namely, their non-linear behavior due to the compressibility of air, friction between the piston and cylinder, and discontinuous flow through control valves [6,7]. Additionally, modeling these systems dynamically is challenging because their air dynamics are often based on empirical assumptions [8]. Achieving precise positioning of pneumatic actuators is also challenging. To expand their range of uses, pneumatic systems must possess the ability to achieve rapid response times and precise positioning control.

System identification (SI) differs from the theoretical approach by relying on observational analysis, rather than fundamental laws of nature, to determine its concepts. SI is a method that can be used to model systems and estimate unknown parameters, as well as to linearize systems to mitigate the limitations of mathematical models [8]. Moreover, this approach proves particularly suitable for complex systems or processes, especially within real-world, practical settings. The goal of SI is to develop a mathematical model that can describe the behavior of a system based on measured input–output data. The process of SI typically involves collecting input–output data from the system and then using these

data to estimate the model parameters. The estimated model can then be used to analyze the system's behavior, predict its response to new inputs, or design a controller to achieve desired performance. The models used in SI can range from simple linear models to more complex non-linear models, and the accuracy of the model depends on the quality and quantity of the input–output data and the complexity of the model. SI is widely used in various fields, including engineering, economics, and biology, to model and control complex systems. It is important to consider the constraints and limitations of the system when designing a controller for practical applications to avoid damaging the system or its components, as well as reducing the control system's performance.

Numerous researchers have been conducting extensive studies in this field, focusing on developing different control strategies for achieving precise pneumatic motion control. These strategies include proportional-integral-derivative (PID) control [1,9,10], sliding mode control (SMC) [11,12], adaptive control [13], fuzzy control [14], and predictive control [15,16].

For this research, the system identification (SI) approach was utilized to obtain the model of the pneumatic system. Additionally, a new control method called fuzzy fractional order proportional integral derivative (Fuzzy FOPID) controller was proposed. The study demonstrated that fractional proportional-integral-derivative (FOPID) controllers offer greater accuracy and flexibility in feedback system adjustment, which can be used to meet more rigorous specifications related to stability phase, gain margins, maximum sensitivity, and performance set point tracking and load disturbance rejection than what is achievable with the conventional PID controller [17–19]. Many researchers have adopted FOPID controllers in recent years because they provide additional features that enhance the durability and success of the system in various applications. Moreover, the investigation results revealed that FOPID is used as a controller in many systems such as motor control systems [20], robotics systems [21], and time-delay systems [22].

Various optimization algorithms have been proposed for tuning controller parameters, including Genetic Algorithm (GA) [23], Cuckoo Search Algorithm (CS) [24], Grey Wolf Optimization (GWO) [25], Gradient-Based Optimization (GBO) [26], and Particle Swarm Optimization (PSO) [27]. GA is a population-based search algorithm inspired by biological evolution. CS is a population-based search algorithm inspired by the behavior of cuckoo birds. GWO is a population-based search algorithm inspired by the social hierarchy of gray wolves. SCA is a population-based search algorithm that simulates the sine and cosine functions. GBO uses the gradient of the cost function to iteratively update the parameter values. PSO is a population-based search algorithm that simulates the movement and interaction of particles. These optimization algorithms have been applied to various control systems and their effectiveness in improving control performance has been demonstrated. However, the choice of algorithm depends on the specific characteristics of the system and the control objectives, and a combination of different algorithms may be necessary to achieve the desired performance. Among these algorithms, PSO was selected for controlling the converter in this study. PSO is inspired by the dynamics of animals moving in groups and builds a solution to the problem by simulating swarm communications [28]. When continuous variables are present, the PSO algorithm presents an effective solution for optimization problems [29].

This research introduces a unique approach to designing a smart pneumatic actuator system through the use of a fuzzy logic control structure. The primary goals and contributions of this study include:

- Developing a two-input-one-output fuzzy controller for the intelligent pneumatic actuator system and assessing its performance in the positioning system. This design incorporates FOPID, which is connected to the output terminal of the fuzzy controller to produce the proposed Fuzzy FOPID controller.
- Utilizing the Particle Swarm Optimization (PSO) technique to identify the optimal values for the suggested controller parameters. Seven parameters are adjusted to achieve the best dynamic behavior for the Fuzzy FOPID controller.

- Validating the superiority of the proposed design by comparing the results obtained from simulations and real-world environments with those of the Fuzzy FOPID.
- Developing a Pneumatic Actuated Ball and Beam System and implementing the Fuzzy FOPID controller on the system.
- Validating the performance of the position controller through both simulation and real-time experiments.

The article is organized into six principal sections. In the second section, the authors describe the process of modeling the IPA system and PABB system. The third section provides a detailed overview of the inner loop controller designs, including Fuzzy PID and Fuzzy FOPID, as well as outer loop designs such as FOPI-FOPD and Fuzzy FOPID. The fourth section of the article focuses on the PSO algorithm. In Section 5, the authors present and analyze the results obtained from the simulation and real-time experiments. Lastly, Section 6 offers a summary of the conclusions drawn from the study.

2. System Modelling

This research aims to create two plant designs: the Intelligent Pneumatic Actuator (IPA) and the ball and beam (BB) system. The IPA model was built using the system identification approach, while the BB model was constructed using mathematical models. These two designs will be utilized in the development of an Intelligent Pneumatic Actuated Ball and Beam System, referred to as IPABBS.

2.1. Intelligent Pneumatic Actuator (IPA) System

2.1.1. IPA Experimental Setup

The setup for the pneumatic cylinder used in this research is shown in Figure 1. The cylinder consists of a guiding rod, an optical encoder, a pressure sensor, and two on/off solenoid valves labeled *V1* and *V2*. The cylinder has a precision of 0.09 mm and can extend up to 200 mm in length. Its operating pressure is 0.6 MPa, with only one chamber controlling the cylinder while the second chamber maintains a constant pressure of 0.6 MPa. Table 1 provides a summary of the different movements that the cylinder can perform.

The movements of the cylinder stroke are based on the conditions of two solenoid valves (*V1* and *V2*). When both valves are off, the cylinder stops. When V1 is off and V2 is on, the cylinder retracts. Conversely, when *V1* is on and *V2* is off, the cylinder extends. Finally, when both valves are on, the cylinder does not move.

The DAQ system and SHC68-68-EPM cable are used to establish communication between the personal computer and the pneumatic actuator system, as depicted in Figure 2.

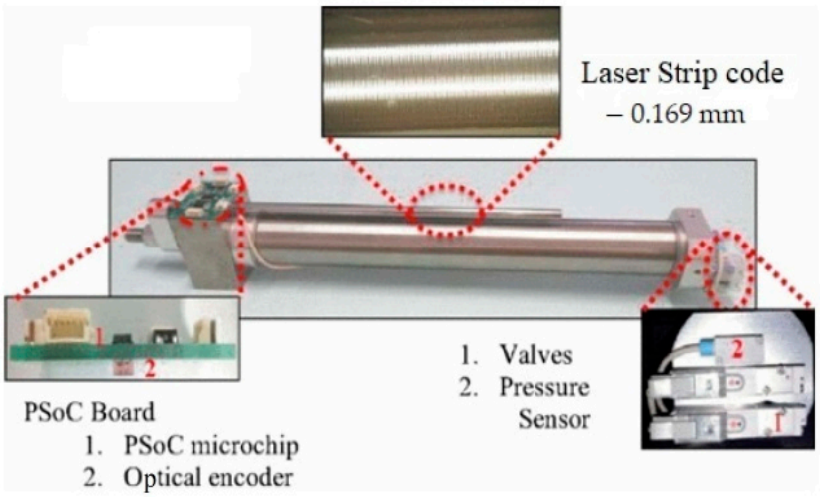

Figure 1. Pneumatic cylinder parts.

Table 1. The PABBS parameters.

Quantity	Value
Beam Length (l)	0.5 m
Pneumatic Actuator Stroke Length (h)	0–200 mm
Angle (α)	Depends on h
The Ball Mass (m)	0.04012 kg
The Ball Radius (R)	0.0107 m
Ball's Moment of Inertia (J)	1.8373 e^{-6}
Gravitational Acceleration (g)	9.8 ms^{-2}

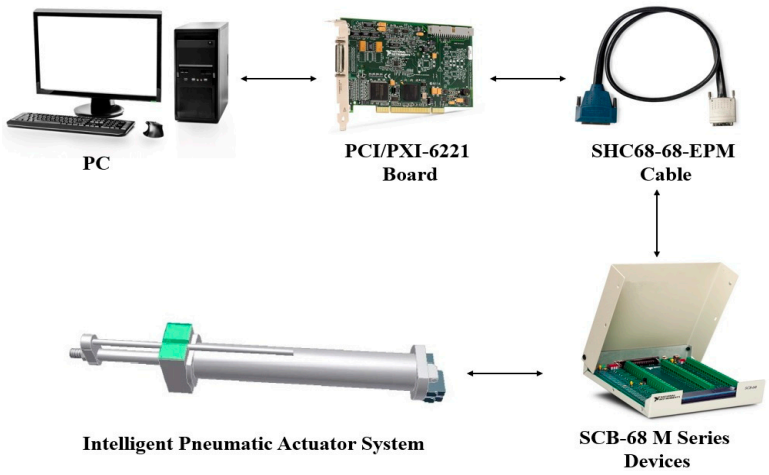

Figure 2. The experimental setup for the IPA system.

2.1.2. System Identification of IPA

To develop an accurate mathematical model of the pneumatic system, a system identification technique was employed in this study. Data were collected through experimentation, resulting in 1600 measurements of input and output data with a sample time (ts) of 10 ms. The collected data was divided into two sets of 800 samples each, with the first set being used for training and the second set for validation. Figure 3 illustrates the plot of input and output data obtained from the real-time experiment.

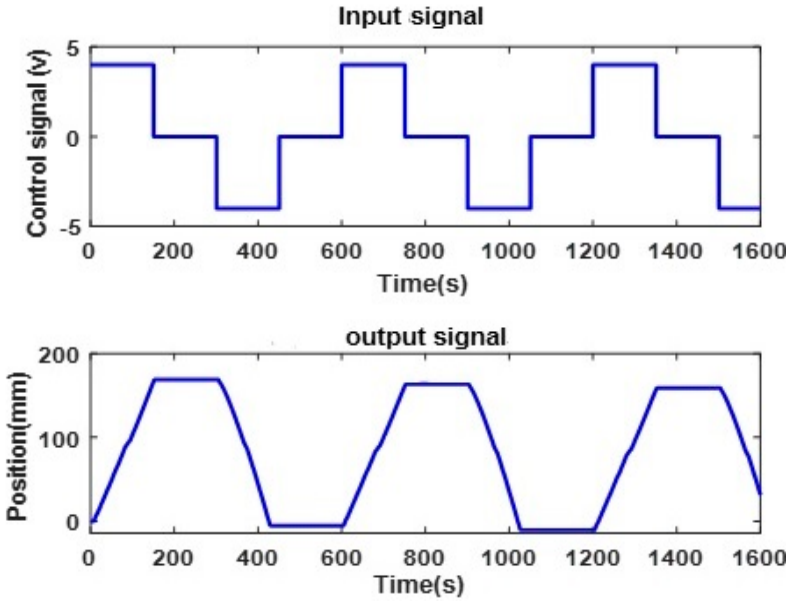

Figure 3. The measured input and output data of the system.

To represent the real system in this study, the ARX331, a third-order linear Autoregressive with Exogenous Input (ARX) model with the order na = 3, nb = 3, and nk = 1, was used. Equation (1) presents the discrete state space equation of the linear third-order ARX.

$$A = \begin{bmatrix} 1.555 & -0.3957 & -0.1593 \\ 1 & 0 & 0 \\ 0 & 1 & 0 \end{bmatrix} \quad B = \begin{bmatrix} 1 \\ 0 \\ 0 \end{bmatrix} \tag{1}$$

$$C = \begin{bmatrix} 0.008 & 0.002 & -0.0012 \end{bmatrix} \quad D = 0$$

Figure 4 displays a comparison between the measured values of the system (represented by a black line) and the output of the simulation model (represented by a blue line). The simulation model was generated using the System Identification Toolbox and has a best fit of 90.75%. The remaining loss of 9.25% could be attributed to factors such as dead zone, air leakage, and friction present in the pneumatic system. The model plant is deemed acceptable since all its poles and zeros are located within the unit circle, as illustrated in Figure 5. Thus, the model is stable and capable of delivering good performance.

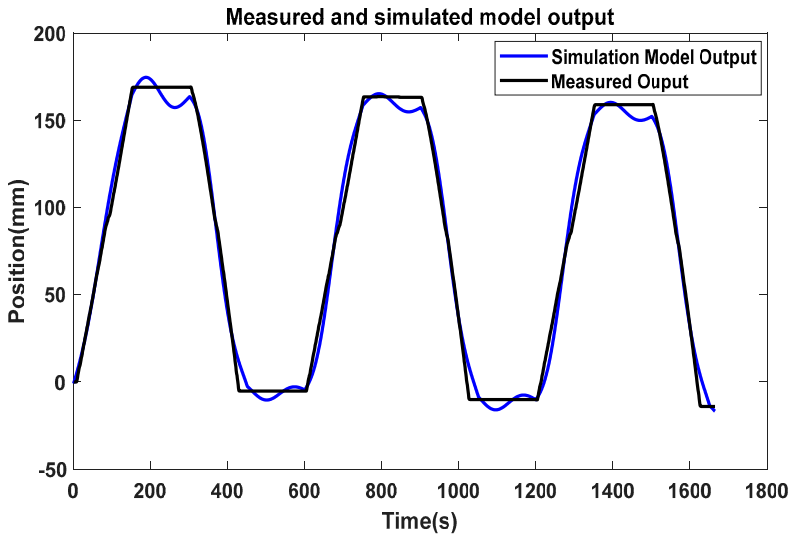

Figure 4. The measured and simulated model output.

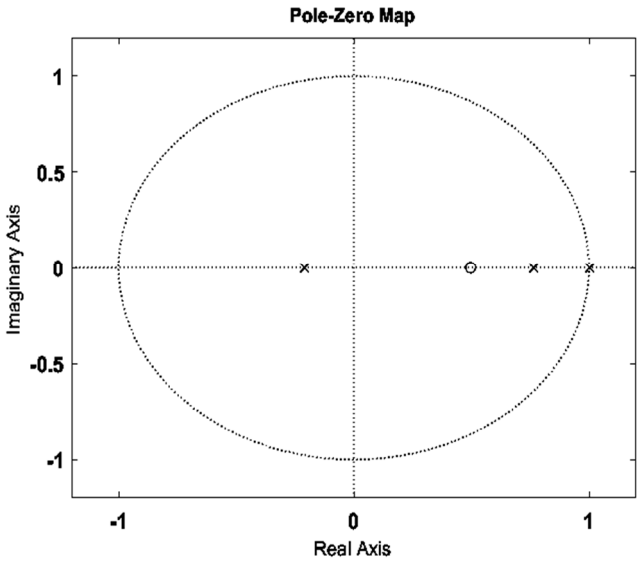

Figure 5. The zeros–poles plot for the model.

2.2. Pneumatic Actuated Ball and Beam (PABB) System

2.2.1. Mathematical Model of Pneumatic Actuated Ball and Beam (PABB) System

The objective of the research is to achieve precise ball placement by regulating the stroke length of the Intelligent Pneumatic Actuator (IPA). In instances where the ball is in an unstable state, adjusting the angle of the beam by moving the pneumatic actuator helps to stabilize the ball. The ball's position is determined by the voltage reading of the resistance sensor, while the beam's angle, which depends on the pneumatic actuator stroke, is determined by the encoder's position. However, controlling the velocity and acceleration of the ball is challenging due to the friction coefficient between the ball and the beam, and directly controlling the stroke of the PA is difficult due to its nonlinearity.

To develop an appropriate controller for the system, it is necessary to derive the system's dynamics equation. Figure 6 illustrates that torque is applied through the right pneumatic actuator at the pivot on the left end, causing the beam to rotate vertically along the y-axis. The ball moves horizontally along the x-axis as the beam moves up and down.

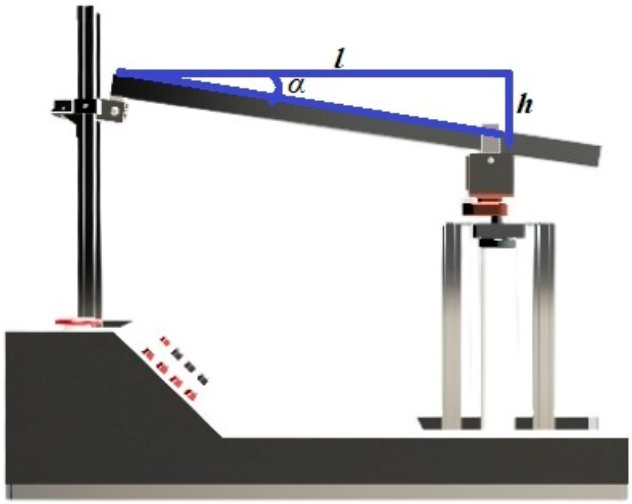

Figure 6. The PABB System.

To streamline and make the model more manageable, all frictional forces have been disregarded. Furthermore, it has been presumed that the ball and the beam remain in constant contact and that there is no slipping during the ball's rolling on the beam. The recommended system parameters can be found in Table 1.

The Lagrangian method has been widely used in model-based research on ball and beam systems with motors [30,31], and it is also used in this study to derive the equation of motion for the ball and beam system. By neglecting friction forces and assuming continuous contact between the ball and beam with no slippage, the resulting Lagrangian equation of motion for the ball can be expressed as follows:

$$\left(\frac{J_b}{r^2} + m\right)\ddot{x} + mg\sin\alpha - mx\left(\dot{\alpha}\right)^2 = 0 \tag{2}$$

Linearization of this equation about the beam angle, $\alpha \approx 0$, gives the following linear approximation of the system:

$$\left(\frac{J_b}{r^2} + m\right)\ddot{x} = -mg\alpha \tag{3}$$

The beam angle can be expressed as in Equation (4).

$$\alpha = \sin^{-1}\frac{h}{l} \tag{4}$$

Equation (4) is linearized using a simple approach where the values of h and l are already known. Figure 7 shows the graph of all possible values obtained by substituting the given values into Equation (4).

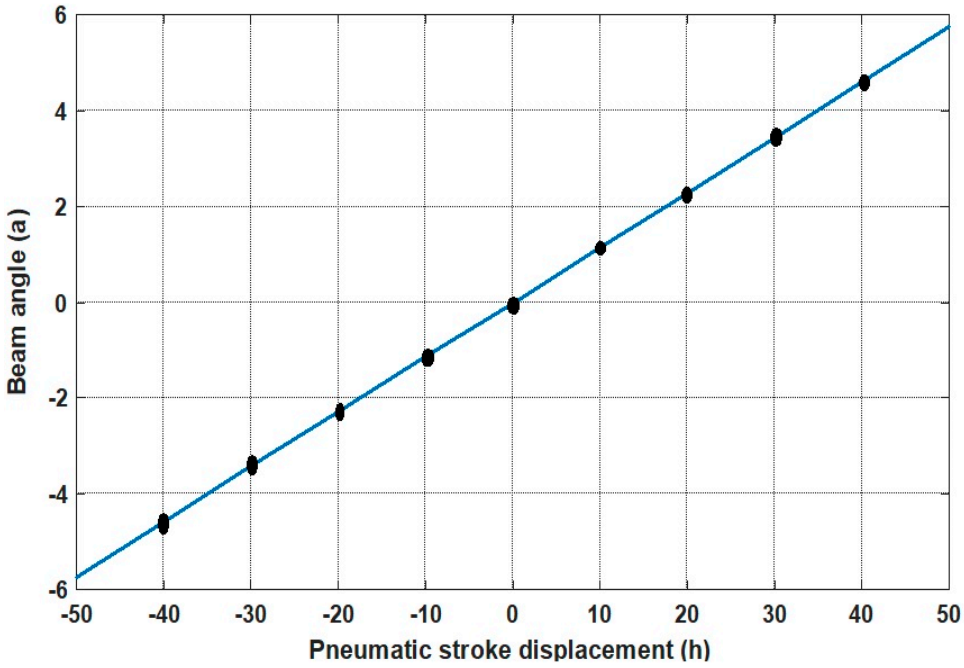

Figure 7. Beam angle vs. Pneumatic stroke displacement graph.

By applying the equation of a straight line to the data presented in Figure 7, one obtains the following equation.

$$\alpha = 0.115\, h \tag{5}$$

Then, by substituting Equation (5) into Equation (3), we obtain

$$\left(\frac{J_b}{r^2} + m\right)\ddot{x} = -0.115\, mgh \tag{6}$$

Taking the Laplace transform of Equation (6), we find

$$\left(\frac{J_b}{r^2} + m\right)X(s)s^2 = -0.115\, mg\, H(s) \tag{7}$$

Rearrange Equation (7), and the transfer function from the pneumatic actuator (H) to the ball position (X) will be obtained.

$$\frac{X(s)}{H(s)} = \frac{-0.115\, mg}{\left(\frac{J_b}{r^2} + m\right)s^2} \tag{8}$$

2.2.2. PABB Experimental Setup

Figure 8 shows the experimental setup designed for the IPA application. The setup consists of several components, including the PABBS structure, compressor, servo-pneumatic actuator, pressure regulator, stainless-steel ball, position sensor (to measure the location of the ball), DAQ card for communication, and PC with MATLAB software.

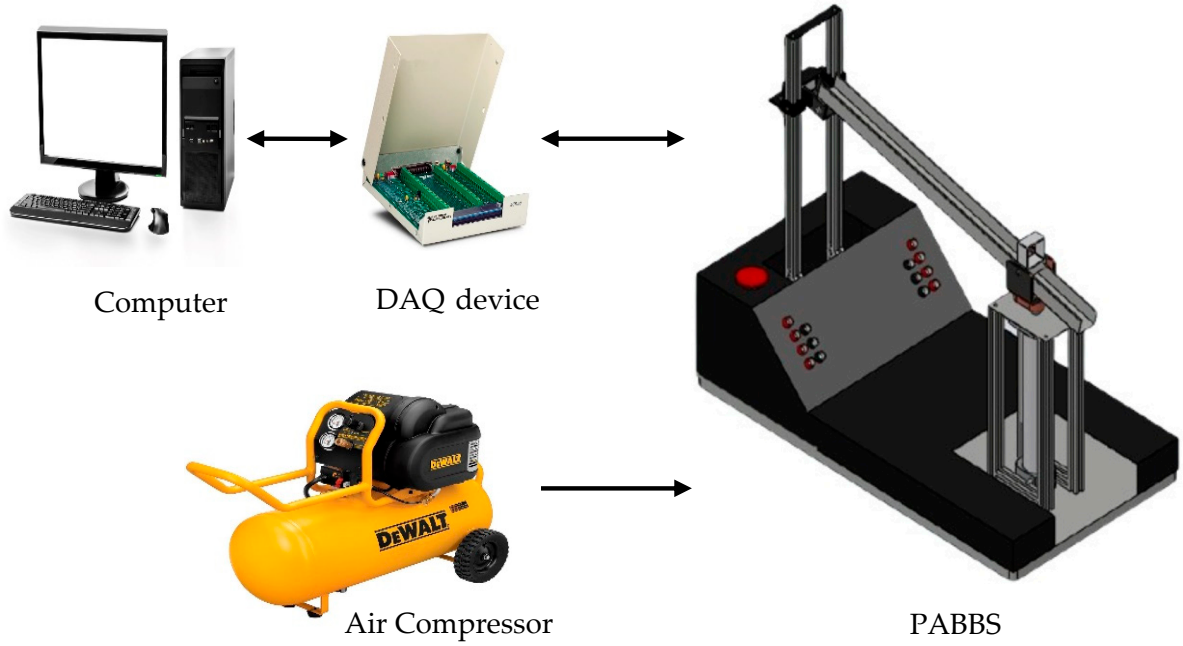

Figure 8. The experimental setup for the PABBS system.

3. Controller Design

This section addresses the controllers' design for both the IPA plant and the ball and beam plant. The control system design for the proposed system comprises two feedback loops: one for the IPA (inner loop) and another for ball position control (outer loop). The inner loop is responsible for controlling the pneumatic stroke length, h, which in turn adjusts the beam angle, α. The inner loop controller is designed with the objective of precisely controlling the IPA's position. On the other hand, the outer loop utilizes the inner feedback loop to regulate the ball's position.

3.1. Intelligent Pneumatic Actuator Controller Design—Inner Loop

This study utilized Fuzzy FOPID and Fuzzy PID controllers to control the intelligent pneumatic actuator, which relies on fuzzy logic control implemented using the fuzzy logic toolbox within the MATLAB/Simulink platform. The fundamental components of fuzzy logic, as presented in Figure 9, include the fuzzifier, rule base, inference engine mapping, and de-fuzzifier [32].

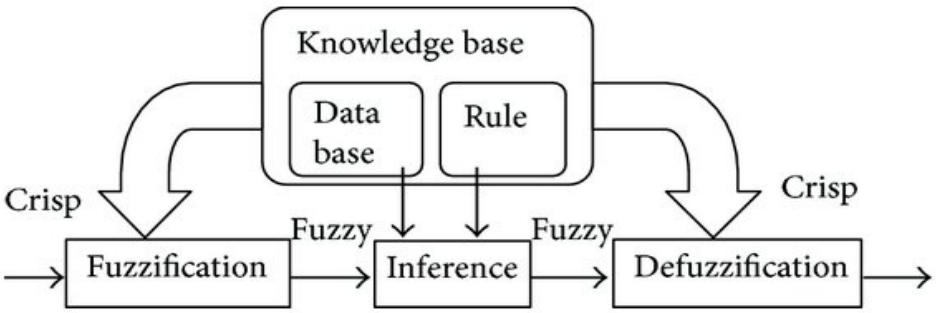

Figure 9. The basic structure of the fuzzy controller.

Figure 10 displays the use of five triangular membership functions, namely Large Negative (LN), Small Negative (SN), Zero (Z), Small Positive (SP), and Large Positive (LP), for input 1 and input 2. The range of MF for input 1 is between −10 and 10, and for input 2 is between −5 and 5, respectively. The output for the fuzzy design is singular, with a linear value, and each variable's value is V2 = −255, V2k = −100, off = 0, V1k = 200, and

V1 = 255. Table 2 shows that 25 rule bases are required to generate the controller's fuzzy output. These rules are derived from a detailed analysis of the dynamic behavior of the pneumatic actuator under investigation because the controller's performance is dependent on them. Furthermore, this design uses the Sugeno-type inference system for fuzzification and the Centroid tool for defuzzification. Figure 11 displays the surface viewer of the Fuzzy controller.

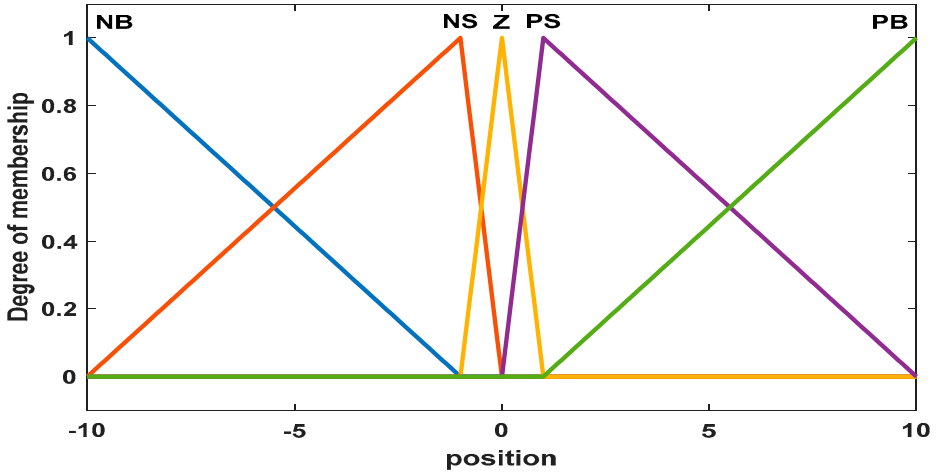

(**a**)

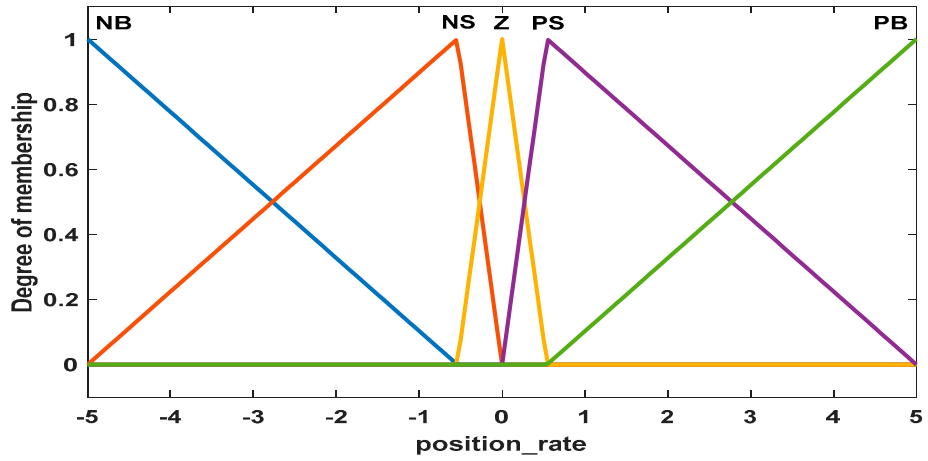

(**b**)

Figure 10. Membership function of (**a**) input1, (**b**) input2.

Table 2. Linguistic rules of the fuzzy controller design.

Error rate, Δe(t)	Error, e(t)				
	NB	NS	Z	PS	PB
NB	NB	NB	NB	PB	PB
NB	NB	NS	NS	PS	PB
NB	NB	NS	Z	PS	PB
NB	NB	NS	PS	PS	PB
NB	NB	NB	PB	PB	PB

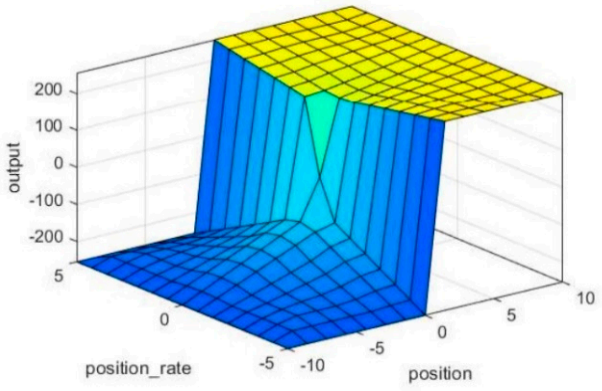

Figure 11. The Fuzzy control surfaces.

3.1.1. The Fuzzy PID (Fuzzy PID) Controller

The PID controller has remained a popular choice in recent times because of its ease of development and installation, as well as its ability to perform well in the presence of system uncertainties [33]. The transfer function for the PID controller can be expressed as shown in Equation (9):

$$C(s) = \frac{U(s)}{E(s)} = K_p + \frac{K_i}{S} + K_d S \quad (9)$$

The system takes three input signals: the error signal, the error derivative signal, and the controller control signal. The error signal is generated by comparing the desired and actual positions of the pneumatic stroke. The error derivative signal is produced by differentiating the error signal, and both signals are inputted into the fuzzy logic controller block and PID controller. The control signal generated by the Fuzzy PID controller is then fed into the pneumatic actuator block to adjust the position of the pneumatic stroke.

The Fuzzy PID controller includes five parameters: K_p, K_i, K_d, K_1, and K_2. The PID parameters (K_p, K_i, and K_d) determine the proportional, integral, and derivative gains of the controller. K_1 and K_2 are the error gain and error rate gain, respectively, which are used to scale the input signals to the fuzzy logic controller block. These parameters can be adjusted to customize the performance of the controller according to the specific requirements of the system. Figure 12 illustrates the structure of a Fuzzy PID controller.

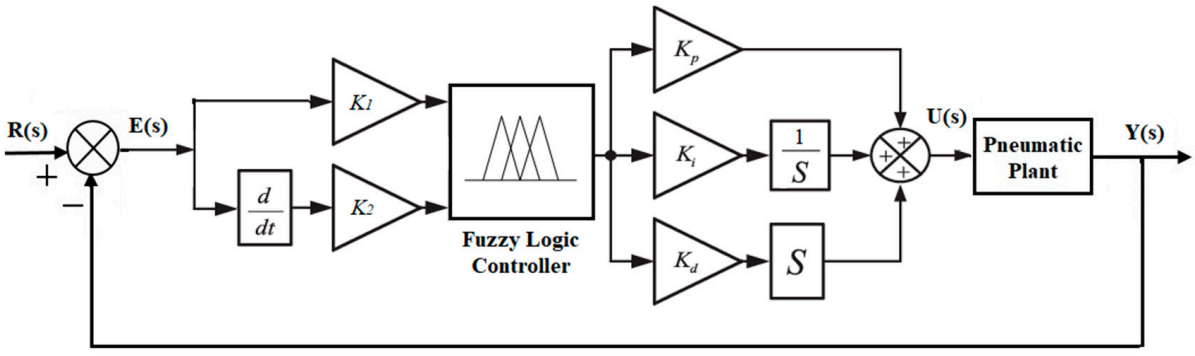

Figure 12. The structure of a Fuzzy PID controller.

3.1.2. The Fuzzy Fractional Order PID (Fuzzy FOPID) Controller

The Fuzzy Fractional Order PID (Fuzzy FOPID) controller is a type of controller used for regulating the position tracking of systems. It combines fuzzy logic with fractional order PID (FOPID) control to improve the system's performance. FOPID control is a type of PID control that uses fractional order calculus to define the proportional, integral, and derivative terms [17]. The fractional order calculus provides more flexibility in designing

the controller to meet specific system requirements. The transfer function for the FOPID controller can be expressed as shown in Equation (10) [18]:

$$C(s) = \frac{U(s)}{E(s)} = K_p + \frac{K_i}{S^{\lambda}} + K_d\, S^{\mu} \tag{10}$$

The Fuzzy FOPID controller is characterized by seven unknown parameters, namely K_p, K_i, K_d, λ, μ, K_1, and K_2. K_p represents the proportional gain, K_i represents the integral gain, K_d represents the derivative gain, λ represents the fractional-order integral, and μ represents the fractional-order derivative. K_1 and K_2 are the error gain and error rate gain, respectively, which scale the input signals to the fuzzy logic controller block. The architecture of a Fuzzy FOPID controller is depicted in Figure 13.

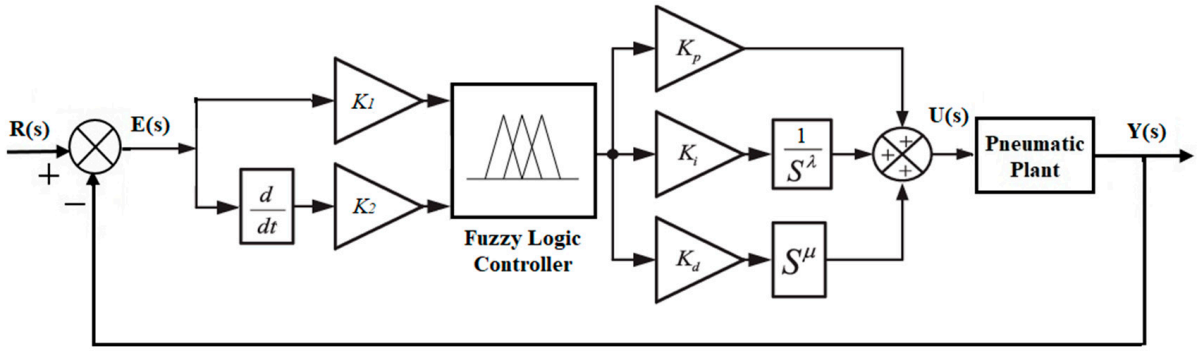

Figure 13. The structure of the Fuzzy FOPID controller.

The effectiveness of the Fuzzy FOPID controller is verified through simulations and real-time experiments. These tests demonstrate that the controller can effectively regulate the position tracking of the system and improve its performance compared to traditional PID controllers. The Fuzzy FOPID controller can be customized to meet the specific requirements of the system by adjusting the scales of fuzzy logic and FOPID.

3.2. PABBS Controller Design—Outer Loop

In this study, two types of controllers were used to regulate the PABB system: Fractional-Order PI–Fractional-Order PD (FOPI-FOPD) controller and Cascade Fuzzy FOPID (CF-FOPID) controller.

3.2.1. Fractional-Order PI–Fractional-Order PD (FOPI-FOPD) Controller Design

The structure proposed in this paper for the FOPI-FOPD controller is depicted in Figure 14. The controller consists of two fractional-order controllers, namely FOPI and FOPD, which are cascaded in series. The control signal for the system is given by Equation (11):

$$C(s) = \frac{U(s)}{E(s)} = \left(K_p + \frac{K_i}{S^{\lambda}}\right).\left(K_{p1} + K_d\, S^{\mu}\right) \tag{11}$$

In order to improve the controller's performance by reducing errors and enhancing transient responsiveness, six parameters need to be adjusted: K_p, K_i, λ, $Kp1$, K_d, and μ. K_p, K_i, and λ represent the proportional gain, integral gain, and fractional-order integral for the FOPI controller, while K_{p1}, K_d, and μ are the proportional gain, derivative gain, and fractional-order derivative, respectively, for the FOPD controller. Figure 14 illustrates the structure of a FOPI-FOPD controller. Adjusting these parameters allows for the optimization of the controller's response to changes in the system's behaviour.

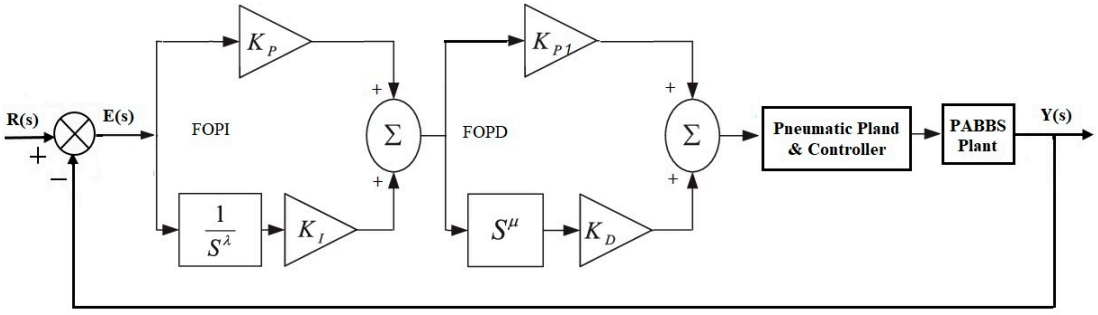

Figure 14. The structure of the FOPI-FOPD controller.

3.2.2. Cascade Fuzzy Fractional-Order PID (CFFOPID) Controller Design

Cascade Fuzzy Fractional-Order PID controller design is a control strategy that combines fuzzy logic with fractional-order calculus to achieve more accurate and flexible control of complex systems. The controller is designed using a cascade structure that allows for the division of the control problem into simpler sub-problems. The basic structure of a CFFOPID controller consists of two stages: the fuzzy logic controller (FLC) stage and the fractional-order PID (FOPID) controller stage. Figure 15 illustrates the structure of a CFFOPID controller.

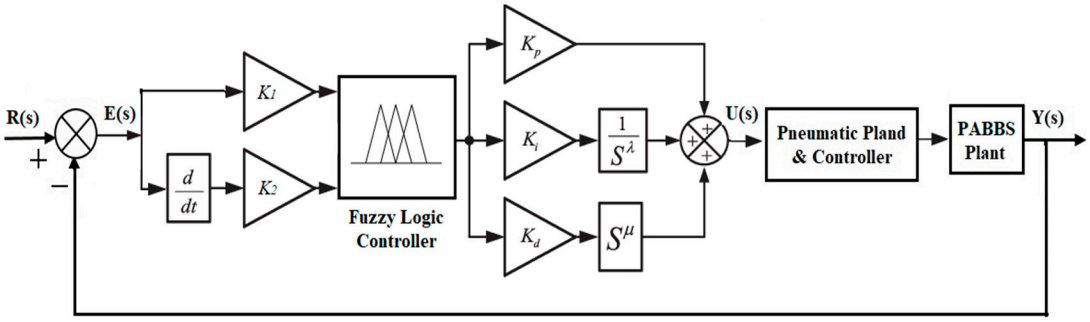

Figure 15. The structure of the CFFOPID controller.

The CFFOPID controller design involves adjusting several parameters, including the gains for the FLC stage, the gains for the FOPID stage, and the fractional-order parameters for the integral and derivative terms.

4. Particle Swarm Optimization Algorithm

In 1995, James and Russell proposed the Particle Swarm Optimization (PSO) algorithm, which is inspired by the collective behavior of birds and has a random probability distribution [34]. PSO is a powerful optimization technique that is particularly effective for solving nonlinear optimization problems. In 1998, an improved version of PSO was introduced by adding an inertia weight coefficient to enhance its performance [35]. PSO is a rule-based algorithm that incorporates both the individual and collective behavior of birds [29,36].

In this approach, every particle in the swarm searches for the best position by continuously updating its location based on its knowledge of the best position it has found so far, as well as the global best position within the swarm. This method is formulated using Equations (12) and (13) for the optimization process [37].

$$v_i(k+1) = W\, v_i(k) + C_1 R_1 (g_{best} - x_i(k)) + C_2 R_2 (p_{best} - x_i(k)) \tag{12}$$

$$x_i(k+1) = x_i(k) + v_i(k+1) \tag{13}$$

$i = 1, 2, \ldots, n$

where v_i is the ith particle velocity, x_i is the ith particle position, k is the iteration number, C_1 and C_2 are the cognitive and social coefficients, w is the inertia weight factor, R_1 and R_2 are random variables of from 0 to 1, p_{best}, i is the individual best position of particle i, g_{best} is the best global position of all the particles in the swarm, and n is the number of birds (particles).

If the condition in (14) is met, then the position is updated through (15):

$$f(x_{ik}) < f(p_{best}) \tag{14}$$

$$x_{ik} = p_{best} \tag{15}$$

where f performs the minimization objective fitness function. The flowchart of the PSO algorithm is illustrated in Figure 16.

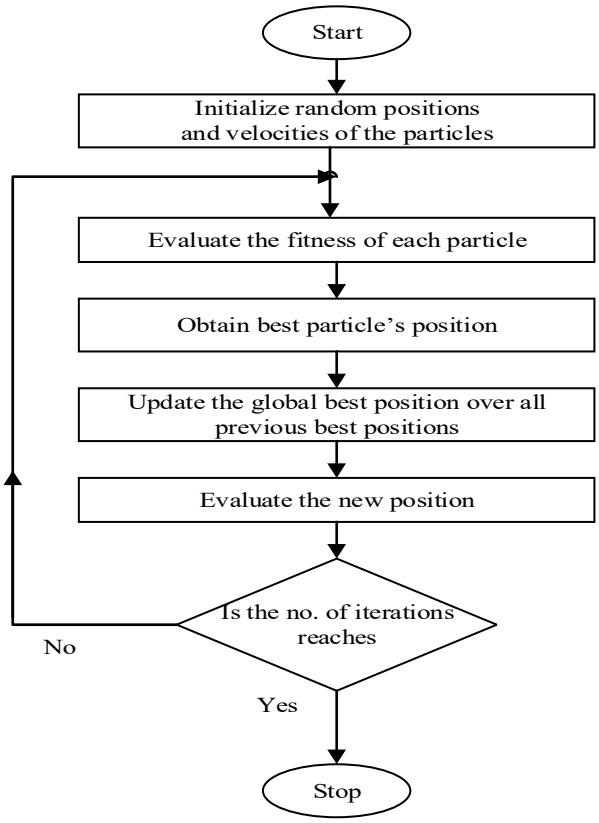

Figure 16. Flow chart of the PSO algorithm.

Typically, optimization methods involve evaluating system performance based on various fitness criteria such as Integral Absolute Errors (IAE), Integral Square Errors (ISE), and Integral Time Square Errors (ITSE). These fitness criteria take into account parameters such as overshoot, rising time, settled time, steady-state error, and the overall tightness of the control system [38]. In this study, the ITSE fitness function as shown in Equation (16) is used to evaluate the performance of the system's output response:

$$ITSE = \int_0^\infty t\, e^2(t).dt \tag{16}$$

Table 3 summarizes the parameters of the PSO algorithm used in this study.

Table 3. The parameters of the PSO algorithm.

Parameter	No. Iteration	No. Particles	Social Coefficient	Cognitive Coefficient	Inertia Weight
Value	30	10	1.42	1.42	0.9

The optimization process for the Fuzzy FOPID-PSO system is illustrated in Figure 17, which includes a block diagram of the process. To find the optimal values of the seven controller parameters, a MATLAB program is used. The program applies a minimization algorithm to search the domain of the particles' position and velocity, and the optimal values of the FOPID controller are obtained in 30 iterations.

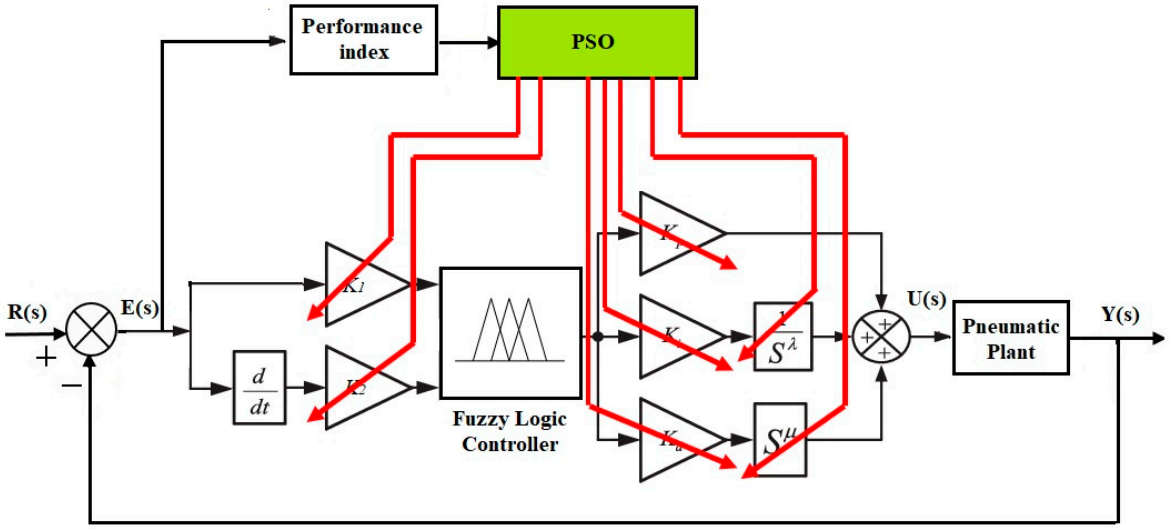

Figure 17. The block diagram of the optimized Fuzzy FOPID controller.

5. Results and Discussion

This part presents the simulation and real-time experimental results for the position control of IPA and PABB systems. The simulation was carried out using a mathematical model of the system, while the real-time experiments were conducted using physical prototypes of the systems. The results of the simulation and experimental tests were compared to evaluate the performance of the position control system. The discussion section provides an analysis of the results and discusses the potential applications of the position control system for IPA and PABB systems.

5.1. Position Control for IPA System

MATLAB-Simulink was utilized as the platform for this research, and Figure 18 displays the Simulink block diagram used for simulation. The controller block in this diagram consists of either a Fuzzy FOPID controller or a Fuzzy PID controller, and the IPA model is represented by Equation (1). Figure 19, on the other hand, illustrates the Simulink block diagram utilized for the real-time experiment setup. The block diagram design consists of five parts, namely the input (position-setpoint), controller, DAQ configuration (I/O), performance index, and output. The input signal used in this experiment is the same as in the simulation, where identical parameters of Fuzzy FOPID and Fuzzy PID controllers were implemented in the real-time experiment for validation purposes.

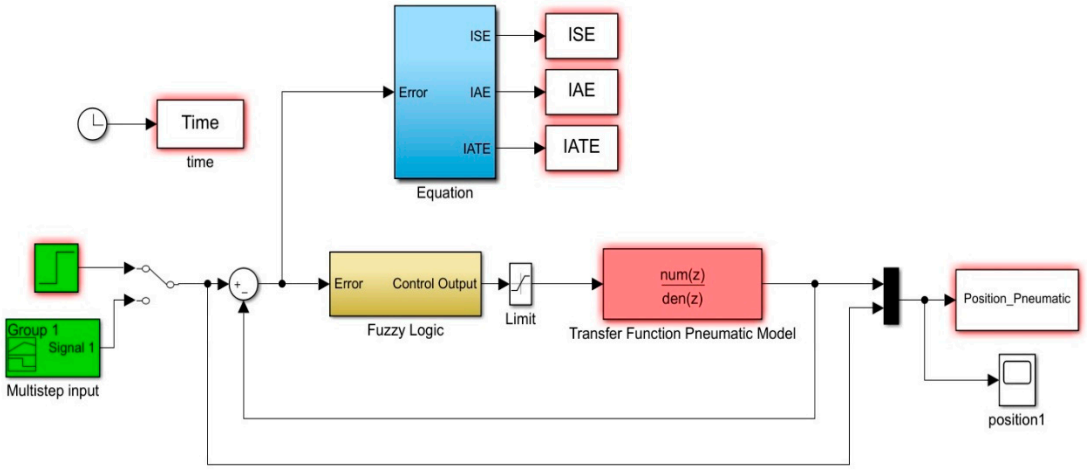

Figure 18. Simulink diagram for IPA simulation.

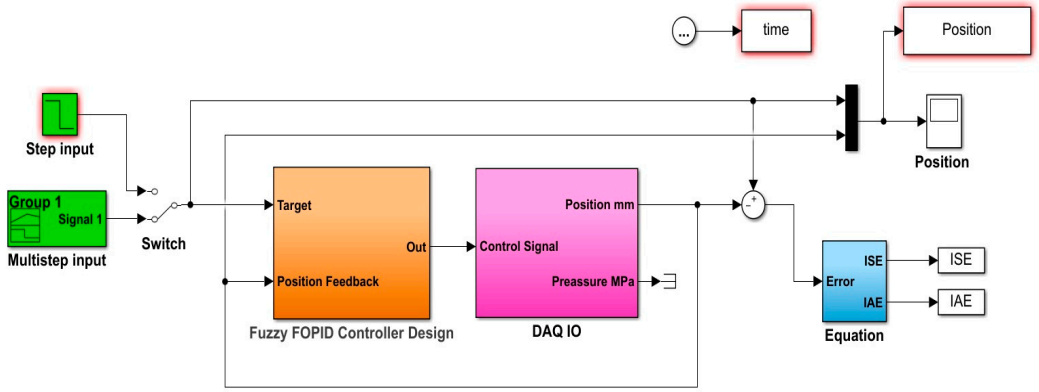

Figure 19. Simulink diagram for IPA real-time experiment.

The ITAE values obtained through successive generations of PSO using the Fuzzy FOPID controller and Fuzzy PID controller are illustrated in Figures 20 and 21, respectively. Table 4 provides a summary of the optimal parameter values found via PSO for both controllers (Fuzzy FOPID and Fuzzy PID).

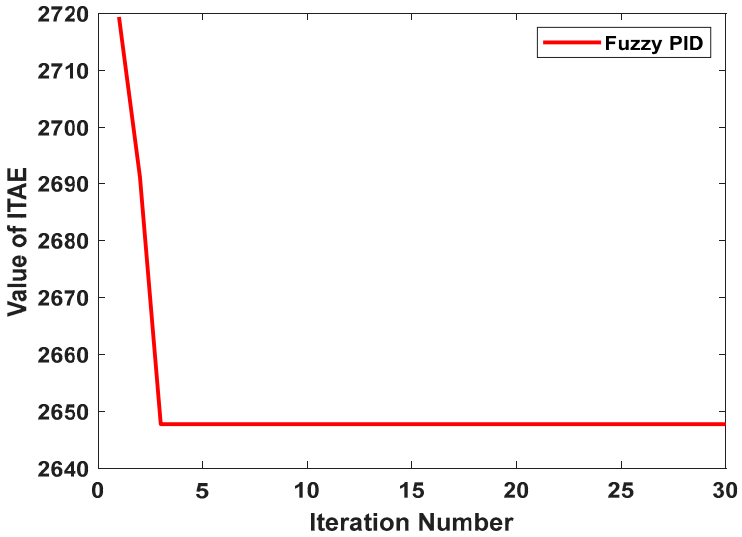

Figure 20. The value of ITAE in successive generations of the PSO Fuzzy PID.

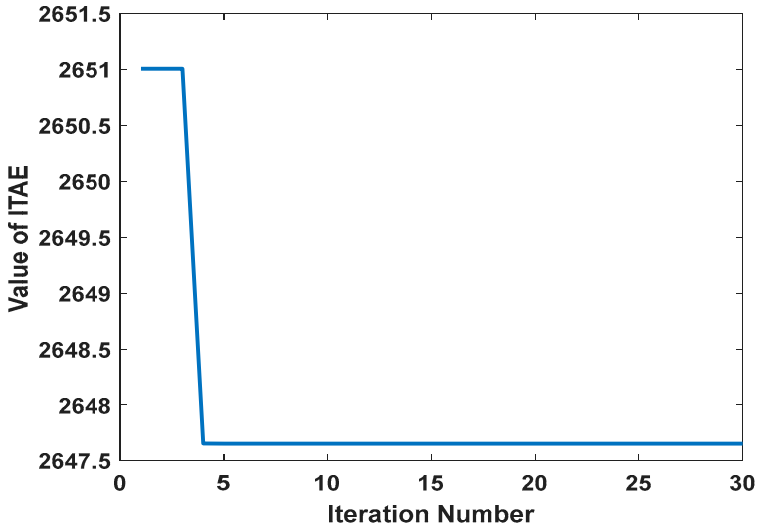

Figure 21. The value of ITAE in successive generations of the PSO Fuzzy FOPID.

Table 4. The optimal values of the controllers.

Criteria	K_1	K_2	K_p	K_i	λ	K_d	μ
Fuzzy FOPID	0.0001	0.0495	25	1	0.1	10	0.1
Fuzzy PID	0.0002	0.05	25	0.1	-	1	-

5.1.1. Simulation Performances of the IPA Positioning System

In this study, the step and multistep trajectories were utilized as reference input signals to evaluate the IPA system's positioning control. Simulation tests were conducted for position step responses with a duration of 15 s and multistep responses with a duration of 25 s, and all the control parameters mentioned in Table 4 were utilized to develop the control system. Two different positioning distances were examined using the step input test, namely mid-stroke (100 mm) and near fully extended (150 mm), where only one valve (Valve 1) of the IPA system was utilized to extend the cylinder stroke. In contrast to the step input test, the multistep input test involved both extension and retraction of the IPA cylinder stroke. Therefore, both Valve 1 and Valve 2, were employed to control the extension and retraction of the IPA cylinder stroke. In Figure 22, the simulation responses of the Fuzzy FOPID controller for step inputs at 100 mm (mid-stroke) and 150 mm (nearly fully extended) are illustrated. On the other hand, Figure 23 displays the multistep response for the Fuzzy FOPID controller. Similarly, Figure 24 showcases the simulation responses of the Fuzzy PID controller for step inputs at 100 mm (mid-stroke) and 150 mm (nearly fully extended), while Figure 25 demonstrates the multistep response for the Fuzzy PID controller. A summary of all the data presented in these figures has been compiled in Table 5.

The data presented in Figures 22–25 along with the information provided in Table 5, indicate that as the distance increased, the rise time (*Tr*) and settling time (*Ts*) of the IPA positioning system also increased steadily. However, the employment of Fuzzy PID resulted in a slightly longer response time compared to Fuzzy FOPID, causing a slower system. To meet the requirements of wider applications, the IPA system should be capable of achieving both fast speed response and accurate positioning control. The inclusion of fractional order parameters in the control signal to the IPA valves using Fuzzy FOPID resulted in a faster and more aggressive speed response compared to Fuzzy PID. Additionally, Fuzzy PID control resulted in a slight overshoot of 0.00022% and 0.00031% for distances of 100 mm and 150 mm, respectively. Furthermore, this study evaluated three performance indices (IAE, ISE, and ITAE) and found that all the controllers produced similar outcomes in terms of the step response. The values of the performance indices for both Fuzzy FOPID and Fuzzy PID controllers were relatively comparable to each other. Specifically,

for IAE, the total error ranged from approximately 39 to 41.1; for ISE, it was around (26–26.6) $\times 10^2$; for ITAE, the Fuzzy FOPID controller had a value of 10.54, while the Fuzzy PID controller had a value of 25.42. On the other hand, Fuzzy FOPID control did not exhibit any overshoot for all distances. All control strategies demonstrated zero steady-state error (e_{ss}) for all distances, indicating that the control system can accurately track the IPA positioning system. This further confirms the effectiveness of the control strategies in achieving accurate positioning control.

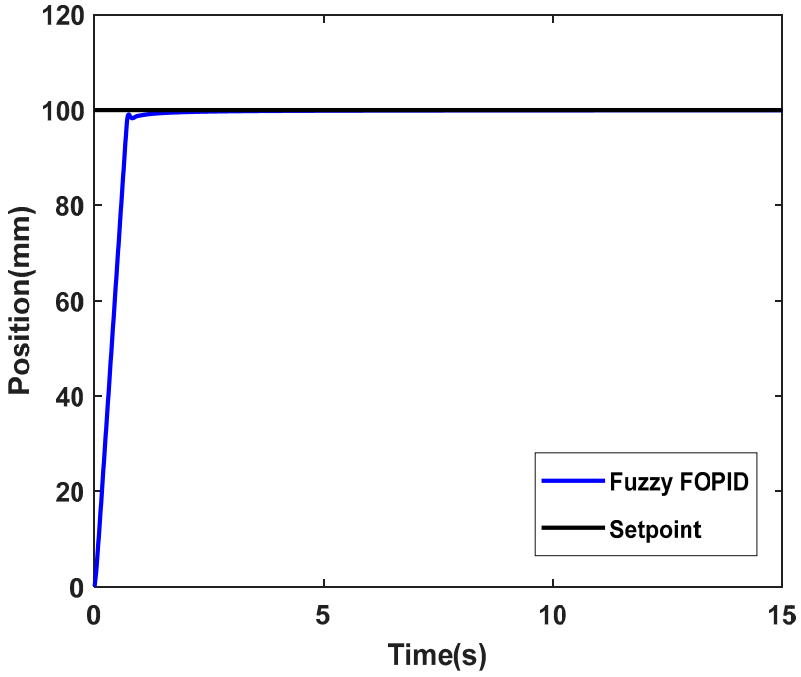

(**a**)

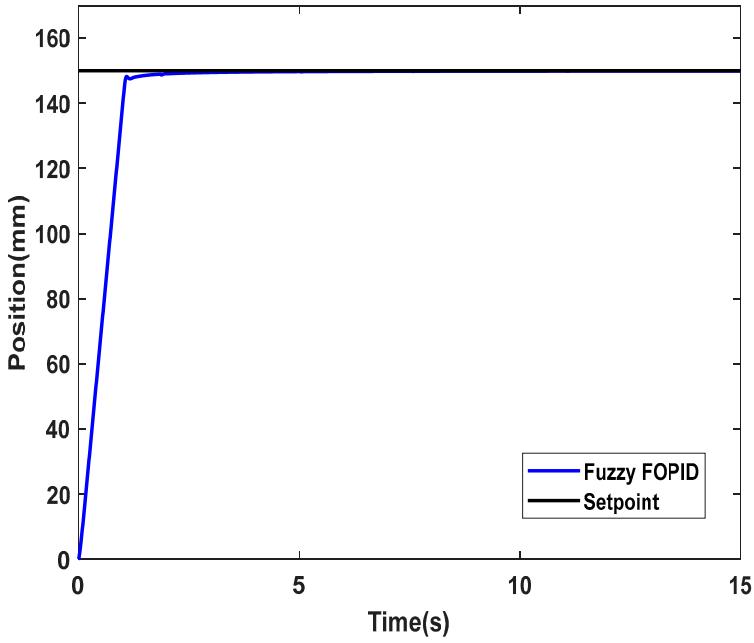

(**b**)

Figure 22. Step response for Fuzzy FOPID simulation at (**a**) 100 mm, (**b**) 150 mm.

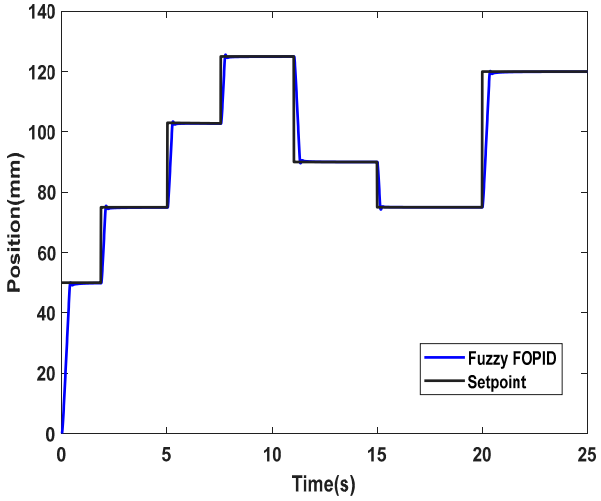

Figure 23. Multistep response for Fuzzy FOPID simulation.

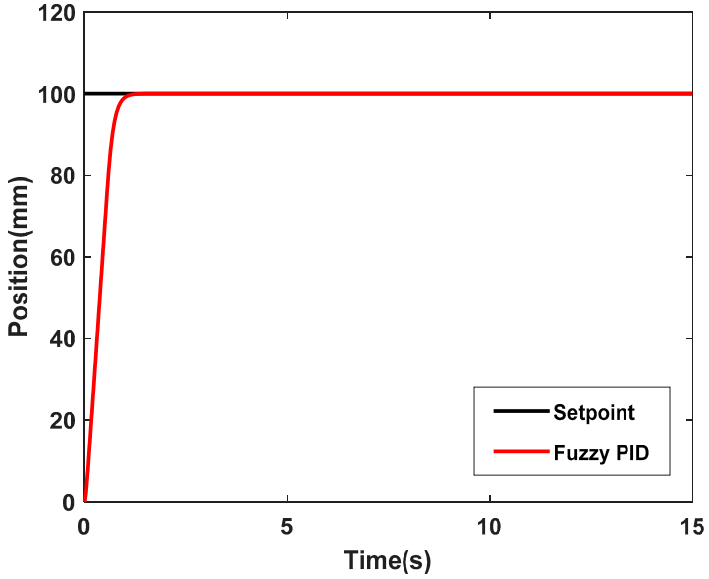

(**a**)

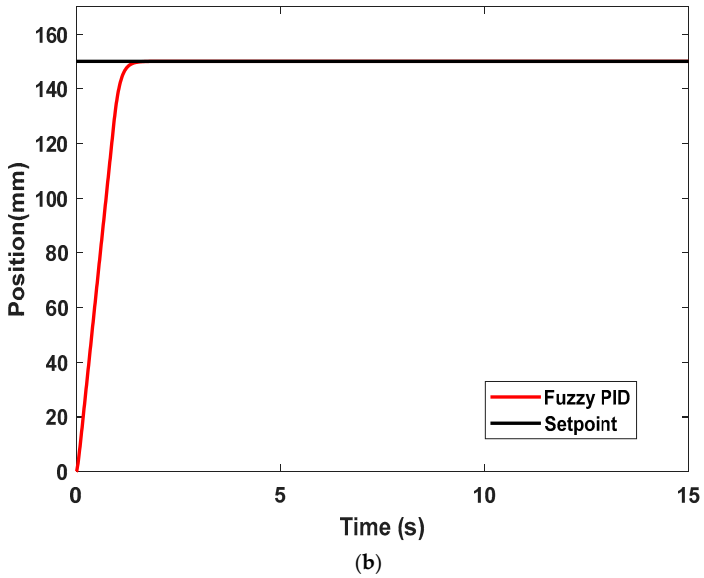

(**b**)

Figure 24. Step response for Fuzzy PID simulation at (**a**) 100 mm, (**b**) 150 mm.

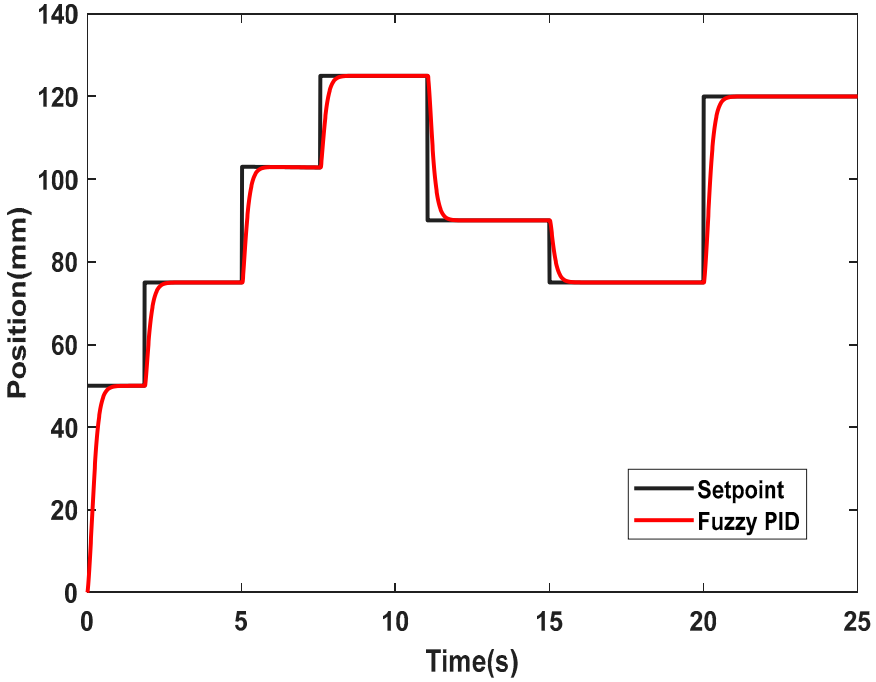

Figure 25. Multistep response for Fuzzy PID simulation.

Table 5. Summary of the step response performances using Fuzzy FOPID and Fuzzy PID.

Distance (mm)	Transient Performance	Fuzzy FOPID	Fuzzy PID
100	*Tr* (s)	0.5616	0.6953
	Ts (s)	0.7188	1.0349
	OS (%)	0	0.00022
	e_{ss}	0	0
150	*Tr* (s)	0.8400	0.9510
	Ts (s)	1.0602	1.2002
	OS (%)	0	0.00031
	e_{ss}	0	0

5.1.2. Experimental Validation Performances of the IPA Positioning System

The research assessed the efficacy of the suggested control approach by conducting several experiments, such as positioning control at different distances and examining the system's robustness to load changes. The performance of the proposed control method was evaluated in each experiment and juxtaposed with established techniques used for comparable pneumatic plant systems to identify enhancements, especially in the IPA positioning system's transient response. A sampling time of 10 ms was used for experimentation, and MATLAB/Simulink was used to develop the proposed control strategy. The simulation test used the same controller parameters to validate the results.

Two position distances (100 mm and 150 mm) and two directions of the cylinder position (horizontal and vertical) were utilized for comparison, and the step signal was applied as the input signal. Each test was carried out for 20 s, and the controller parameters used in the simulation test were the same. The performance of the Fuzzy FOPID system's transient response, including the rise time (*Tr*), settling time (*Ts*), overshoot (*OS*), and steady-state error (e_{ss}), in controlling the IPA positioning system at all distances were then compared with that of the Fuzzy PID. Figure 26 offers a comparative analysis of the step tests conducted with the cylinder positioned horizontally, and the distance of the position

was adjusted between fully retracted (0 mm) and nearly fully retracted (100 mm). Similarly, Figure 27 provides a comparative view of the step tests, with the cylinder position being horizontal and the position distance adjusted between fully retracted (0 mm) and nearly fully extended (150 mm). The findings from both figures are summarized in Table 6.

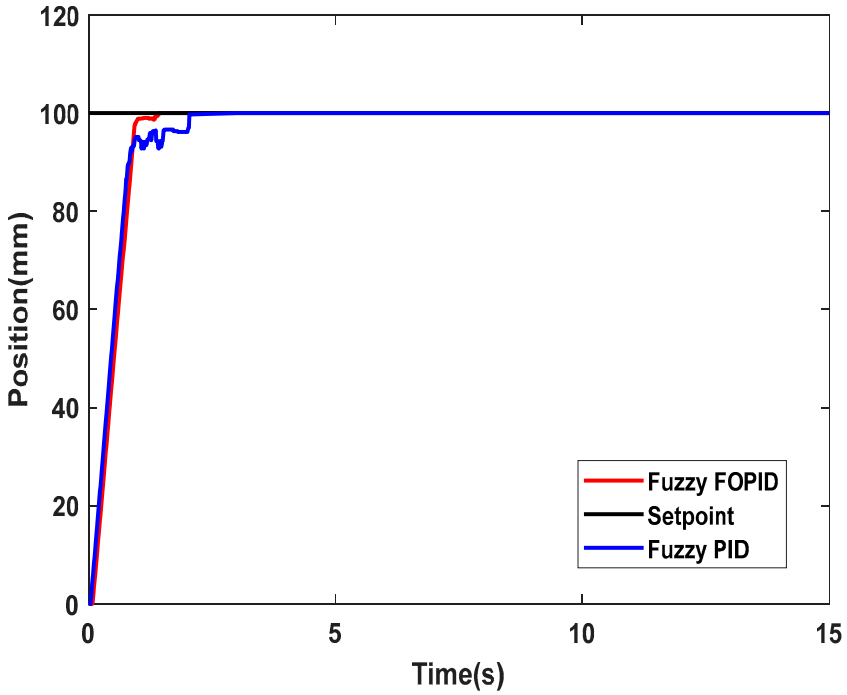

Figure 26. Experimental step response at 100 mm for the horizontal position.

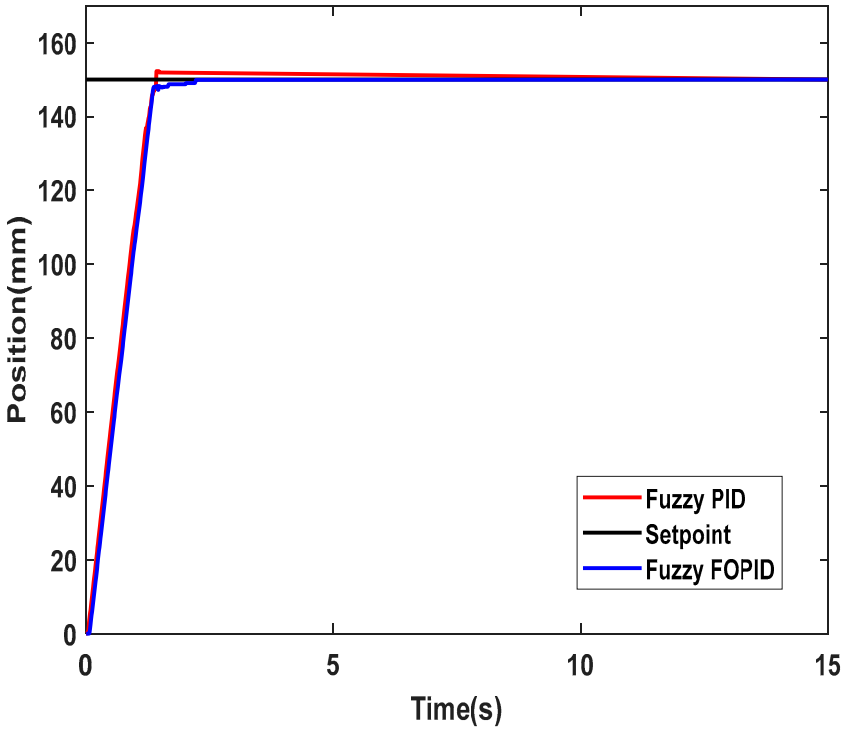

Figure 27. Experimental step response at 150 mm for the horizontal position.

Table 6. Summary of the experimental response using different control strategies for the horizontal position.

Distance (mm)	Transient Performance	Fuzzy FOPID	Fuzzy PID
100	*Tr* (s)	0.6577	0.7418
	Ts (s)	0.9544	1.0337
	OS (%)	0	0.00022
	e_{ss}	0	0
150	*Tr* (s)	1.0468	1.0301
	Ts (s)	1.3497	1.3741
	OS (%)	0	0.00031
	e_{ss}	0	0

Figure 28 compares the step tests for the vertical cylinder position, with the position distance ranging from fully retracted (0 mm) to almost fully retracted (100 mm), whereas Figure 29 compares the step tests for the vertical cylinder position, with the position distance ranging from fully retracted (0 mm) to almost fully extended (150 mm). The outcomes from Figures 9 and 10 are consolidated in Table 7 for reference.

The experimental results presented in Figures 26–29, as well as Tables 6 and 7, illustrate a noticeable increase in both rise time (*Tr*) and settling time (*Ts*) of all control strategies as the distance to be covered by the cylinder stroke increases. In other words, the farther the distance, the longer it takes for the control strategies to achieve their steady-state value. The comparison of the control strategies reveals that Fuzzy FOPID outperforms the others in achieving precise control of the IPA cylinder stroke at both 100 mm and 150 mm positioning distances. Furthermore, the Fuzzy FOPID controller outperformed conventional controllers by demonstrating no overshoot and steady-state inaccuracy. In addition, the IAE, ISE, and ITAE of the Fuzzy FOPID are less than those of the Fuzzy PID. The Fuzzy FOPID controller improved the system's transient response by 12.78%, 24.25%, and 100% in rise time, settling time, and overshoot, respectively, compared to the results obtained from the Fuzzy PID controller. As a result, the outcomes obtained from utilizing the Fuzzy FOPID controller are deemed satisfactory. The controller exhibited a significant enhancement in the transient response performance by offering a faster response without overshooting for all position distances.

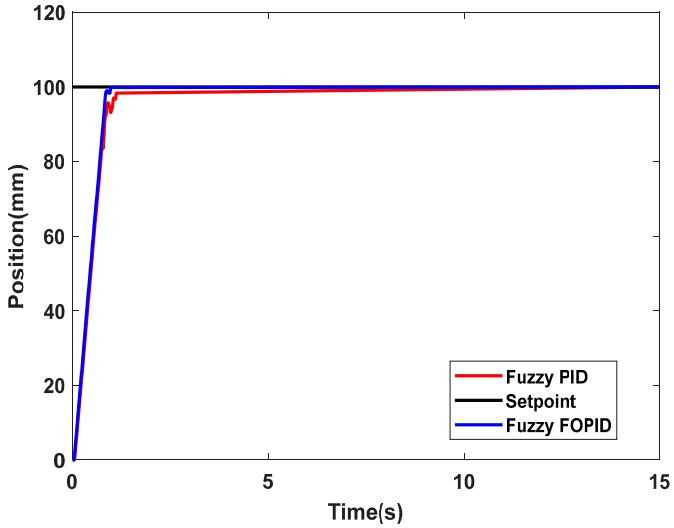

Figure 28. Experimental step response at 100 mm for the vertical position.

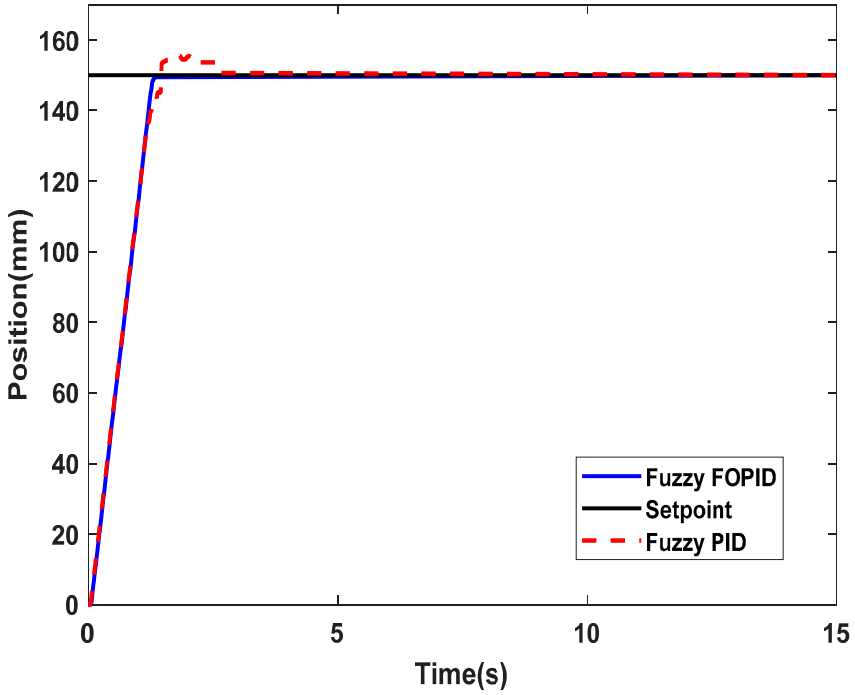

Figure 29. Experimental step response at 150 mm for the vertical position.

Table 7. Summary of the experimental response using different control strategies for the vertical position.

Distance (mm)	Transient Performance	Fuzzy FOPID	Fuzzy PID
100	*Tr* (s)	0.6372	0.7306
	Ts (s)	0.8381	1.1076
	OS (%)	0	0.00022
	e_{ss}	0	0
150	*Tr* (s)	0.9874	1.0196
	Ts (s)	1.2726	1.5662
	OS (%)	0	0.00031
	e_{ss}	0	0

Moreover, the IPA system's positioning performance for horizontal and vertical positions using Fuzzy PID and Fuzzy FOPID strategies with a multistep trajectory as the input signal is depicted in Figures 30 and 31, respectively.

When developing a controller, robustness is a crucial factor that must be considered. A controller is considered robust if it can compensate for any changes in the system due to external loads. This study examined the effect of varying loads on controller robustness. The IPA positioning system was subjected to a step response with mid-stroke positions (100 mm and 150 mm), and different external loads (1 kg, 3 kg, 6 kg, and 8 kg) were attached to the end of the cylinder stroke for each test, which lasted 20 s. The controller parameters used in this test were the same as those used in the unloading condition. The experimental performance of the vertical IPA positioning system's response to varying loads, controlled by the Fuzzy FOPID, is illustrated in Figures 32 and 33. Moreover, the performance details are presented in Table 8.

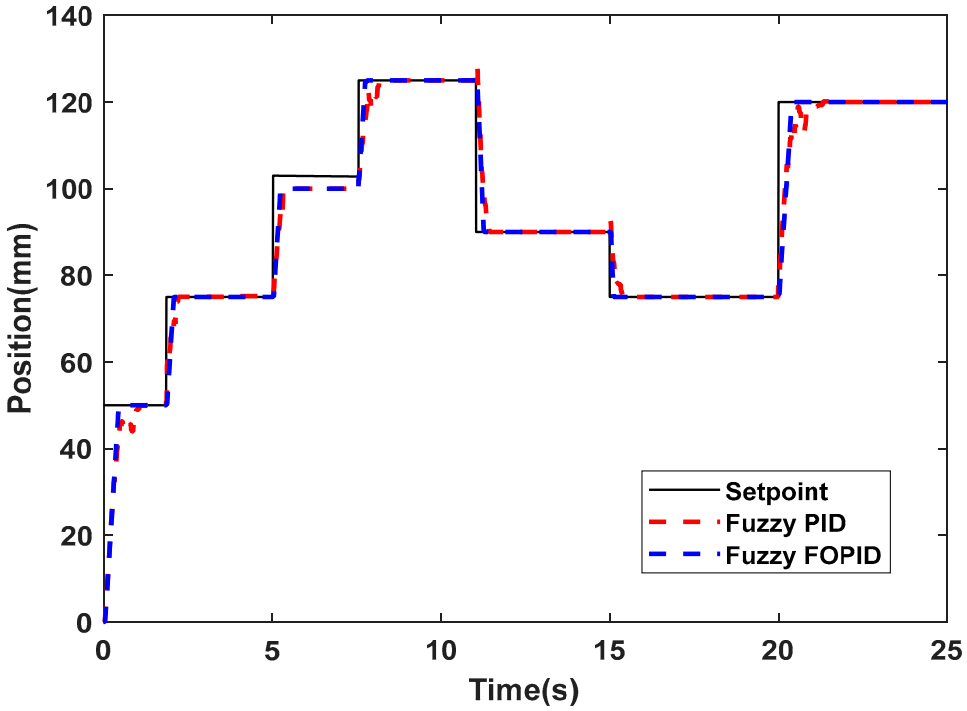

Figure 30. Experimental multistep response for the horizontal position.

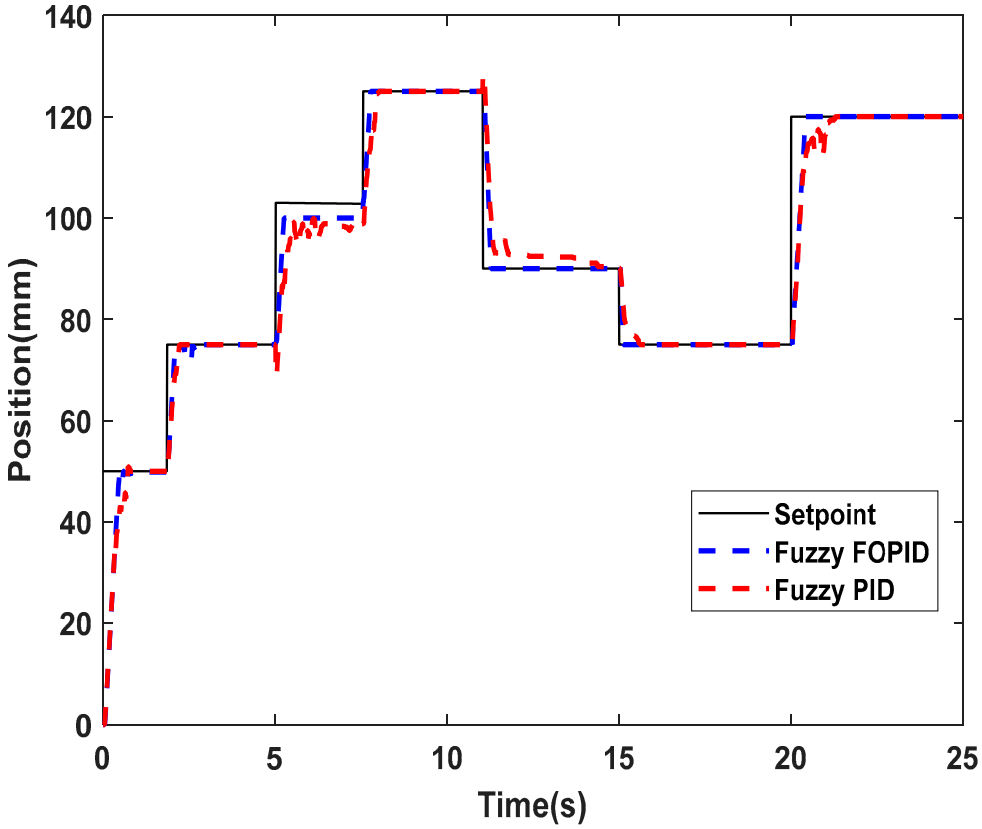

Figure 31. Experimental multistep response for the vertical position.

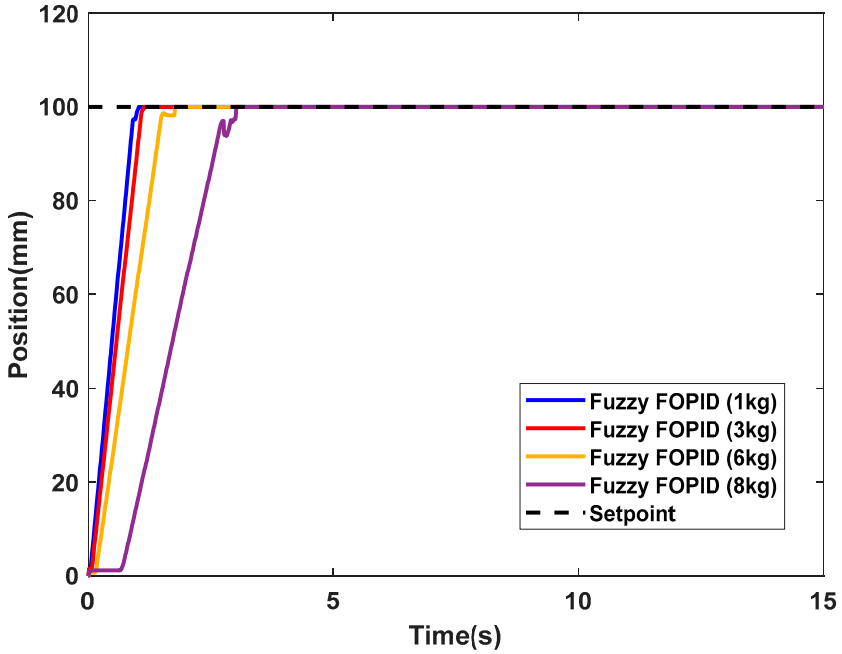

Figure 32. Experimental step response based on load variation at 100 mm.

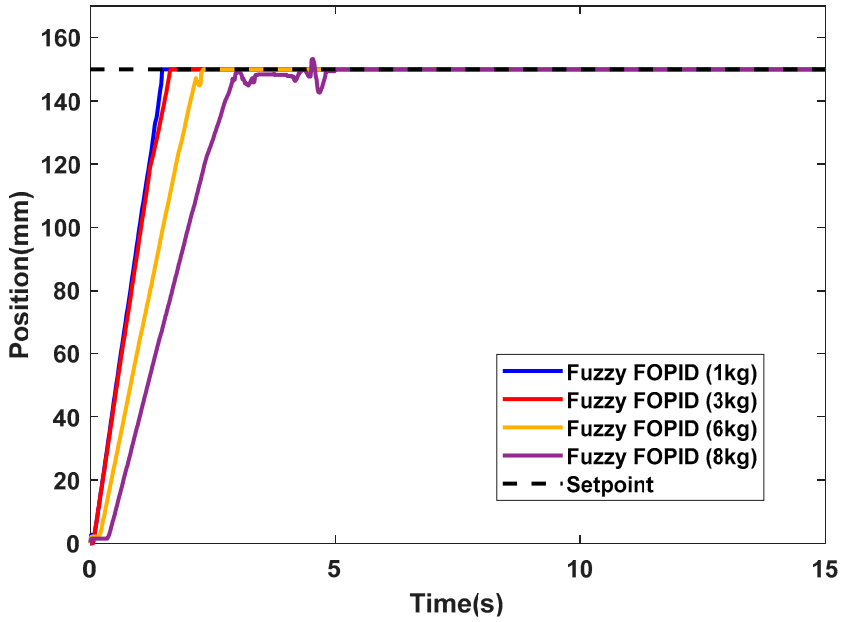

Figure 33. Experimental step response based on load variation at 150 mm.

Table 8. Summary of the experimental response using different loads.

Loads (kg)	Fixed Position at 100 mm		Fixed Position at 150 mm	
	Rise Time Tr (s)	Settling Time Ts (s)	Rise Time Tr (s)	Settling Time Ts (s)
1	0.7199	0.9763	1.1513	1.4590
3	0.8290	1.0781	1.2435	1.6047
6	1.1002	1.4944	1.6076	2.2613
8	1.6912	3.0097	2.0625	4.7827

Furthermore, Figure 34 demonstrates the positioning performances of the IPA system using the Fuzzy FOPID strategy, considering the multistep trajectory as an input signal to the IPA system, with load variations.

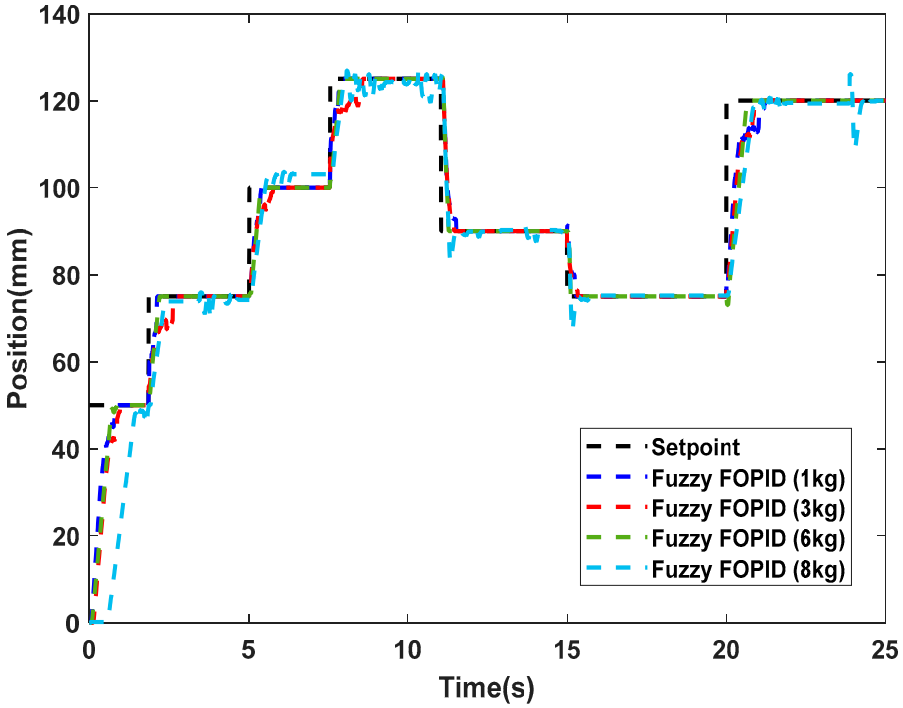

Figure 34. Experimental multistep response based on load variation.

Table 8 and Figure 34 present the results of the experimental evaluation of the performance of the pneumatic actuator controlled via Fuzzy FOPID under different loads and fixed positions. The data presented in the table show the rise time and settling time for the IPA system when the load is varied from 1 kg to 8 kg at fixed positions of 100 mm and 150 mm. The data show that the performance of the system decreases as the load increases, particularly for the fixed position at 150 mm. At 6 kg, the rise time and settling time for both fixed positions are still within acceptable limits. However, at 8 kg, the rise time and settling time for the fixed position at 150 mm are significantly higher, indicating a deterioration in performance. This suggests that the maximum load capacity and performance of the pneumatic actuator should be considered when designing and implementing a control system for the actuator.

5.2. PABB System Application Results

This research employed MATLAB-Simulink as the platform, and the Simulink block diagrams used for the PABB system simulation and the real-time experiment setup are shown in Figures 35 and 36, respectively. The controller block in Figure 35 comprises a Fuzzy FOPID or a FOPI-FOPD controller, while the PABB system model is represented by Equation (1). Figure 36 shows the block diagram design, which includes five parts: input (position-setpoint), controller, DAQ configuration (I/O), performance index, and output. The input signal used in the experiment is the same as in the simulation, and identical parameters of Fuzzy FOPID and FOPI-FOPD controllers were used for validation purposes.

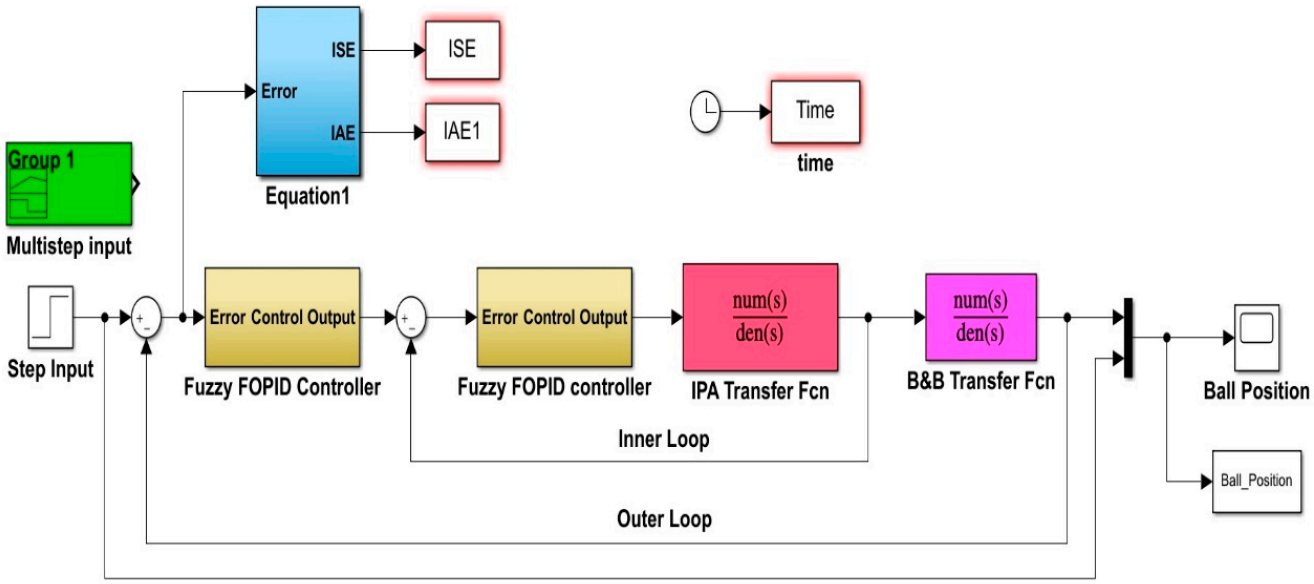

Figure 35. Simulink diagram for PABB system simulation.

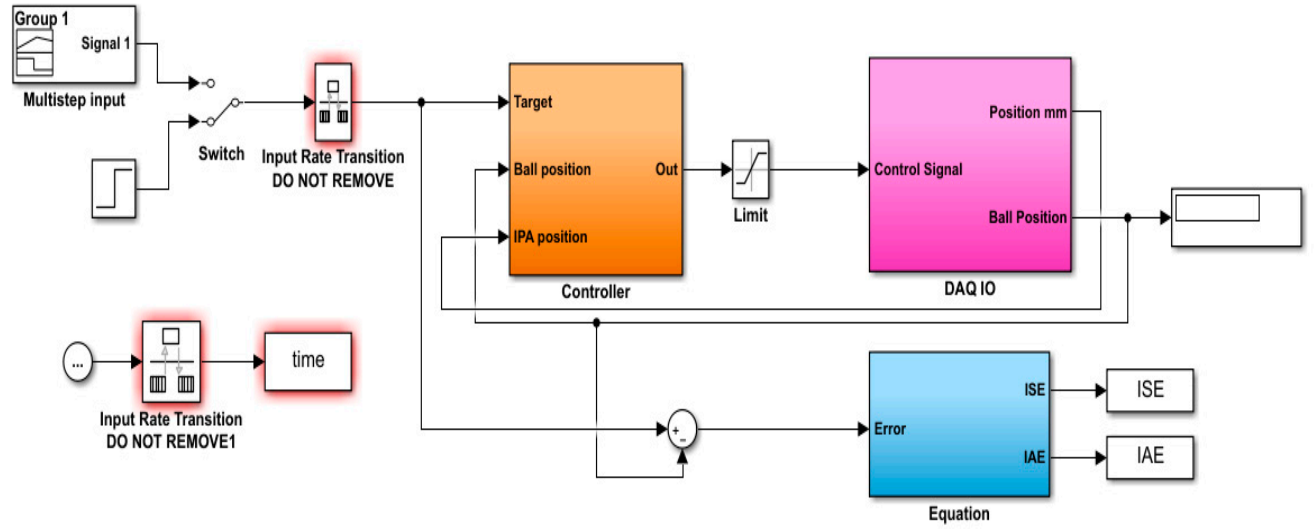

Figure 36. Simulink diagram for PABB system real-time experiment.

5.2.1. Simulation Performances of the PABB System

The PABB system's positioning control was evaluated using step and multistep trajectories as reference input signals in this study. Simulation tests were conducted for both position step responses (15 s) and multistep responses (25 s), with all the control parameters mentioned in Table 9 utilized to develop the control system.

Table 9. The optimal values of Fuzzy FOPID and FOPI-FOPD controllers.

Criteria	K_1	K_2	K_p	K_{pi}	K_{pd}	K_i	λ	K_d	μ
Fuzzy FOPID	0.0495	0.0001	0.1	-	-	0.15	1	1	0.1
FOPI-FOPD	-	-	-	1	1	0.01	0.1	1	1

Figure 37 shows the simulation results, which indicate that both the FOPI-FOPD and Fuzzy FOPID controllers are capable of tracking the target input. The Fuzzy FOPID controller achieves the setpoint faster than the FOPI-FOPD controller. Both controllers

exhibit consistent and rapid responses while regulating the movement of the ball, with no overshoot and only minor steady-state error. In addition, the FOPI-FOPD controller had an ISE value of 8.233×10^4, an IAE value of 403.4, and an IATE value of 423. The Fuzzy FOPID controller had a slightly lower ISE value of 6.036×10^4, an IAE value of 252.6, and an IATE value of 875, indicating better performance compared to the FOPI-FOPD controller. The Fuzzy FOPID controller outperforms the FOPI-FOPD controller, as evidenced by the better results displayed in Table 10.

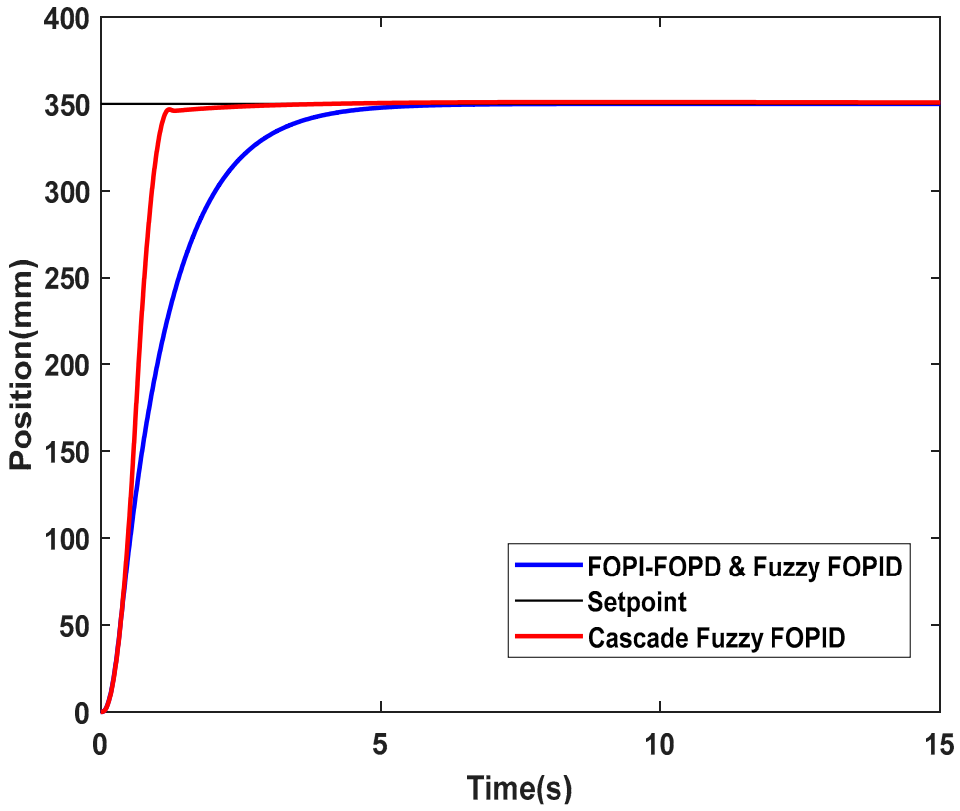

Figure 37. Simulated step responses for Fuzzy FOPID and FOPI-FOPD.

Table 10. Summary of the simulated response of the PABB system.

Controllers	Performance Index			
	Rise Time *Tr* **(s)**	**Settling Time** *Ts* **(s)**	**Overshoot** *OS* **(%)**	**Steady-State Error** e_{ss} **(%)**
FOPI-FOPD	2.091	3.910	0.0055	0
Cascade Fuzzy FOPID	0.6682	1.1359	0.2768	0

Following that, a multistep input was employed to assess the stability and performance of the controllers. Both the FOPI-FOPD and Fuzzy FOPID controllers performed almost identically, smoothly controlling the ball. The results of the multistep response are shown in Figure 38.

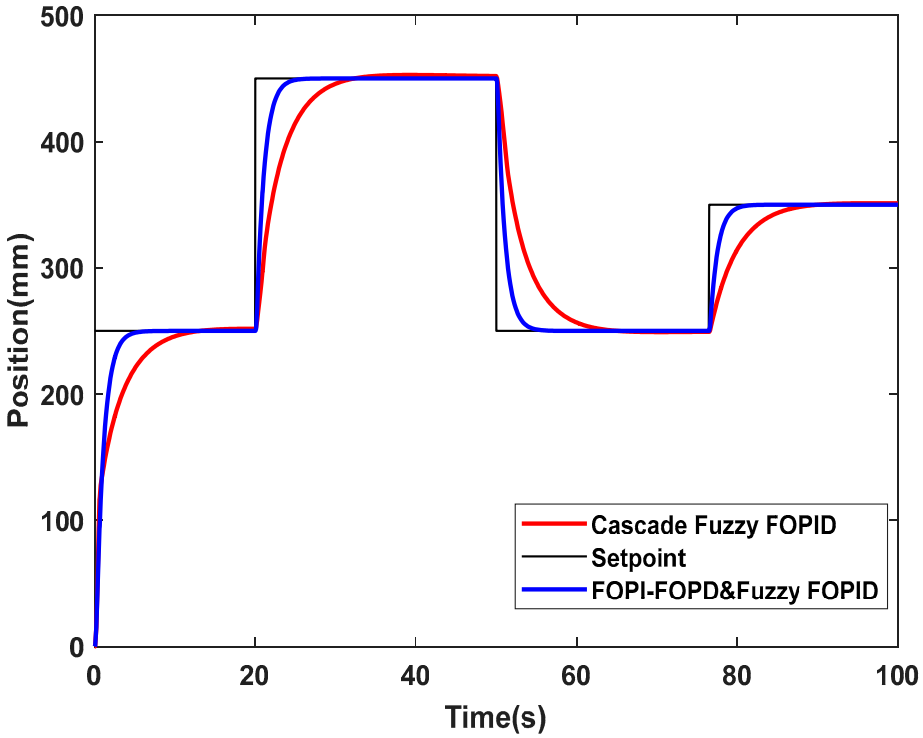

Figure 38. Simulated multistep responses for Fuzzy FOPID and FOPI-FOPD.

5.2.2. Experimental Validation Performances of the PABB System

To prevent the ball from moving too quickly, which could complicate regulation, the pneumatic actuator stroke, h, is restricted to a range of +50 mm (upward) and −50 mm (downward). At the outset of the experiment, h is set to 100 mm. This configuration ensures that the pneumatic system can execute the necessary up-and-down movements.

The controllers are designed using a simulation environment and a mathematical model of the PABB system. The experimental verification of the FOPI-FOPD controller and the Cascade Fuzzy FOPID controller is demonstrated in Figure 39. Table 11 provides a summary of the outcomes from the step response analysis, revealing that the ball's position control experiences increased oscillations as a result of the pneumatic movement's impact. However, due to several factors such as changes in nonlinear characteristics caused by air compressibility, valve dead zone issues, high friction forces, and noise generated by position sensors, the experimental results exhibit slight variations from the simulation outcomes. Despite these challenges, the PABB system yields a favorable outcome in which the primary objective of the system is accomplished. The proposed system can effectively regulate the position and balance of the ball.

Table 11. Summary of the experimental response of the PABB system.

Controllers	Performance Index			
	Rise Time *Tr* **(s)**	**Settling Time** *Ts* **(s)**	**Overshoot** *OS* **(%)**	**Steady-State Error** e_{ss} **(%)**
FOPI-FOPD Fuzzy FOPID	0.3710	10.7986	35.5380	1.3520
Cascade Fuzzy FOPID	0.8235	4.9381	9.8500	0

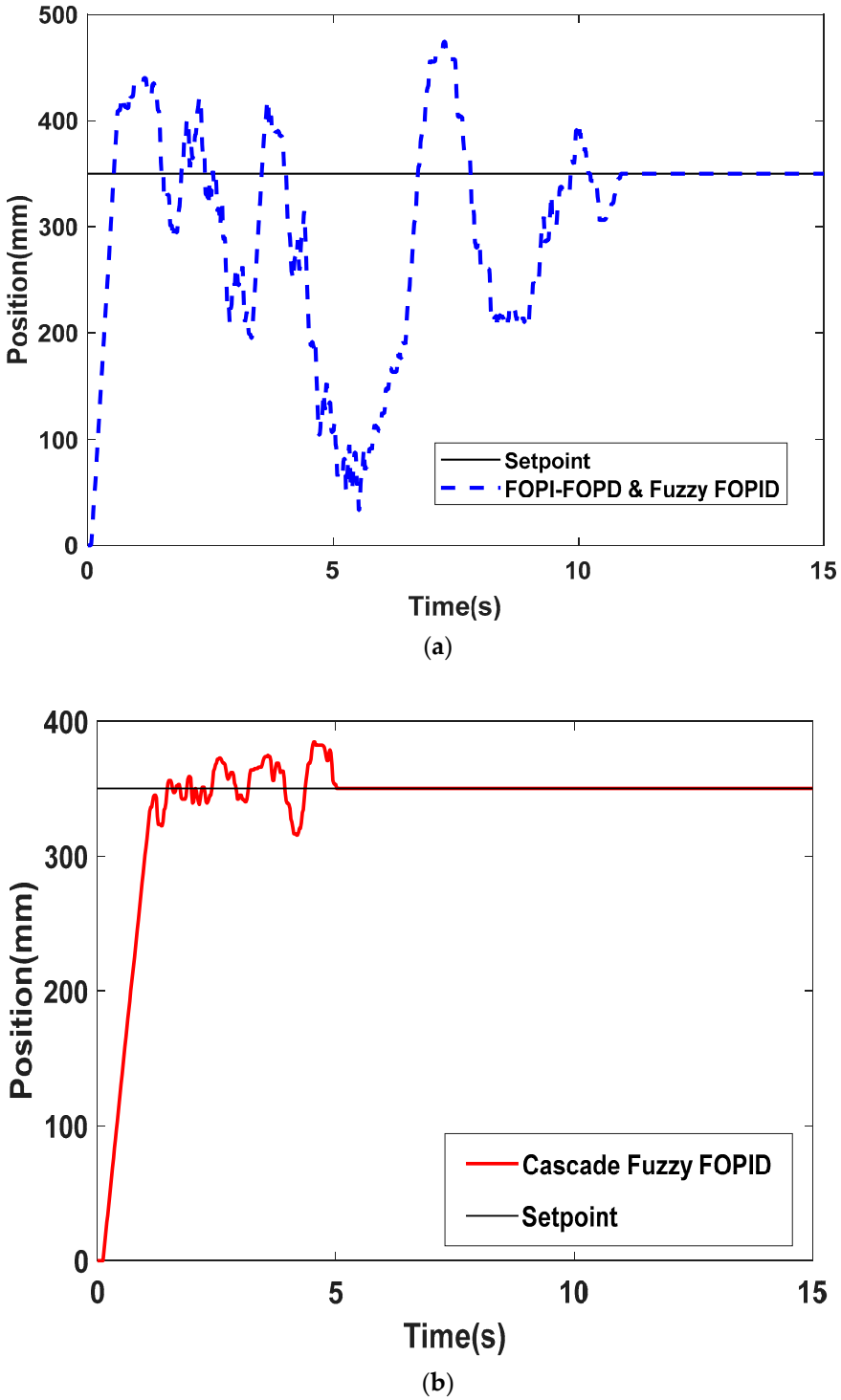

Figure 39. Experimental step responses for (**a**) Fuzzy FOPID and (**b**) FOPI-FOPD.

6. Conclusions

The primary objective of this study was to develop and evaluate a Fuzzy FOPID controller for an intelligent pneumatic actuator (IPA) system to achieve accurate positional control. The study utilized the ARX model to simulate the pneumatic system and the PSO technique to determine the optimal values for the seven controller parameters required to achieve the best dynamic behavior for the Fuzzy FOPID controller. The results indicated that the Fuzzy FOPID controller outperformed the Fuzzy PID controller in terms of stability, robustness, fast response, and zero steady-state error. The study then applied the model

and controller of the pneumatic actuator to the pneumatically actuated ball and beam (PABB) system using two control loops for inner and outer positioning. The Cascade Fuzzy FOPID controller was found to provide a quick and smooth response in controlling the ball's motion. The study validated the performance of the position controller through both simulation and real-time experiments, which demonstrated the effectiveness of the proposed Fuzzy FOPID controller in achieving precise and stable positional control in pneumatic systems.

Author Contributions: Conceptualization, M.N.M., A.A.M.F., S.S. and S.M.; Methodology, M.N.M., A.A.M.F., S.S. and S.M.; Software, M.N.M.; Validation, M.N.M.; Formal analysis, M.N.M.; Investigation, M.N.M., A.A.M.F. and S.S.; Resources, M.N.M., A.A.M.F., S.S. and S.M.; Data curation, M.N.M., A.A.M.F., S.S. and S.M.; Writing—original draft, M.N.M.; Writing—review & editing, A.A.M.F., S.S. and S.M.; Supervision, A.A.M.F., S.S. and S.M.; Project administration, M.N.M. and A.A.M.F.; Funding acquisition, A.A.M.F., S.S. and S.M. All authors have read and agreed to the published version of the manuscript.

Funding: This research received no external funding.

Data Availability Statement: Not applicable.

Acknowledgments: The research has been carried out under program Research Excellence Consortium (JPT (BPKI) 1000/016/018/25 (57)) with the title Consortium of Robotics Technology for Search and Rescue Operations (CORTESRO) provided by Ministry of Higher Education Malaysia (MOHE). The authors also acknowledge Universiti Teknologi Malaysia (UTM) under vote no (4L930) for the facilities and support to complete this research.

Conflicts of Interest: The authors declare no conflict of interest.

References

1. Van Varseveld, R.B.; Bone, G.M. Accurate position control of a pneumatic actuator using on/off solenoid valves. *IEEE/ASME Trans. Mechatron.* **1997**, *2*, 195–204. [CrossRef]
2. Taghizadeh, M.; Najafi, F.; Ghaffari, A. Multimodel PD-control of a pneumatic actuator under variable loads. *Int. J. Adv. Manuf. Technol.* **2010**, *48*, 655–662. [CrossRef]
3. Rahmat, M.F.; Salim, S.N.S.; Faudzi, A.A.M.; Ismail, Z.H.; Samsudin, S.I.; Sunar, N.H.; Jusoff, K. Non-linear modeling and cascade control of an industrial pneumatic actuator system. *Aust. J. Basic Appl. Sci.* **2011**, *5*, 465–477.
4. Qian, P.; Pu, C.; Liu, L.; Lv, P.; Ruiz Páez, L.M. A novel pneumatic actuator based on high-frequency longitudinal vibration friction reduction. *Sens. Actuators A Phys.* **2022**, *344*, 113731. [CrossRef]
5. Saravanakumar, D.; Mohan, B.; Muthuramalingam, T. A review on recent research trends in servo pneumatic positioning systems. *Precis. Eng.* **2017**, *49*, 481–492. [CrossRef]
6. Faudzi, A.M.; Osman, K.; Rahmat, M.F.; Mustafa, N.D.; Azman, M.A.; Suzumori, K. Nonlinear mathematical model of an Intelligent Pneumatic Actuator (IPA) systems: Position and force controls. In Proceedings of the 2012 IEEE/ASME International Conference on Advanced Intelligent Mechatronics (AIM), Kaohsiung, Taiwan, 11–14 July 2012; pp. 1105–1110. [CrossRef]
7. Chen, H.M.; Shyu, Y.P.; Chen, C.H. Design and Realization of a Sliding Mode Control Scheme for a Pneumatic Cylinder X-Y Axles Position Servo System. *IET* **2010**, 416–421. [CrossRef]
8. Muftah, M.N.; Xuan, W.L.; Athif, A.; Faudzi, M. ARX, ARMAX, Box-Jenkins, Output-Error, and Hammerstein Models for Modeling Intelligent Pneumatic Actuator (IPA) System. *J. Integr. Adv. Eng.* **2021**, *1*, 81–88. [CrossRef]
9. Gentile, A.; Giannoccaro, N.I.; Reina, G. Experimental tests on position control of a pneumatic actuator using on/off solenoid valves. *Proc. IEEE Int. Conf. Ind. Technol.* **2002**, *1*, 555–559. [CrossRef]
10. Osman, K.; Faudzi, A.A.M.; Rahmat, M.F.; Mustafa, N.D.; Abidin, A.F.Z.; Suzumori, K. Proportional-integrative controller design of Pneumatic system using particle swarm optimization. In Proceedings of the 2013 IEEE Student Conference on Research and Development, Putrajaya, Malaysia, 16–17 December 2013; pp. 421–426. [CrossRef]
11. Tsai, Y.C.; Huang, A.C. Multiple-surface sliding controller design for pneumatic servo systems. *Mechatronics* **2008**, *18*, 506–512. [CrossRef]
12. Azahar, M.I.P.; Irawan, A.; Ismail, R.M.T.R. Self-tuning hybrid fuzzy sliding surface control for pneumatic servo system positioning. *Control Eng. Pract.* **2021**, *113*, 104838. [CrossRef]
13. Schindele, D.; Aschemann, H. Adaptive friction compensation based on the LuGre model for a pneumatic rodless cylinder. In Proceedings of the 2009 35th Annual Conference of IEEE Industrial Electronics, Porto, Portugal, 3–5 November 2009; pp. 1432–1437. [CrossRef]
14. Azman, M.A.; Osman, K.; Natarajan, E. Integrating Servo-Pneumatic Actuator with Ball Beam System based on intelligent position control. *J. Teknol.* **2014**, *3*, 73–79. [CrossRef]

15. Mu, S.; Goto, S.; Shibata, S.; Yamamoto, T. Intelligent position control for pneumatic servo system based on predictive fuzzy control. *Comput. Electr. Eng.* **2019**, *75*, 112–122. [CrossRef]
16. Osman, K.; Faudzi, A.; Athif, M.; Rahmat, M.F.; Hikmat, O.F.; Suzumori, K. Predictive Functional Control with Observer (PFC-O) Design and Loading Effects Performance for a Pneumatic System. *Arab. J. Sci. Eng.* **2015**, *40*, 633–643. [CrossRef]
17. Muftah, M.N.; Athif, A.; Faudzi, M.; Sahlan, S.; Shouran, M. Modeling and Fuzzy FOPID Controller Tuned by PSO for Pneumatic Positioning System. *Energies* **2022**, *15*, 3757. [CrossRef]
18. Podlubny, I. Fractional-order systems and PIλDμ controllers. *IEEE Trans. Automat. Contr.* **1999**, *44*, 208–214. [CrossRef]
19. Sikander, A.; Thakur, P.; Bansal, R.C.; Rajasekar, S. A novel technique to design cuckoo search based FOPID controller for AVR in power systems. *Comput. Electr. Eng.* **2018**, *70*, 261–274. [CrossRef]
20. Rajasekhar, A.; Kumar Jatoth, R.; Abraham, A. Design of intelligent PID/PIλDμ speed controller for chopper fed DC motor drive using opposition based artificial bee colony algorithm. *Eng. Appl. Artif. Intell.* **2014**, *29*, 13–32. [CrossRef]
21. Dumlu, A.; Erenturk, K. Trajectory tracking control for a 3-DOF parallel manipulator using fractional-order PIλDμ control. *IEEE Trans. Ind. Electron.* **2014**, *61*, 3417–3426. [CrossRef]
22. Luo, Y.; Chen, Y. Stabilizing and robust fractional order PI controller synthesis for first order plus time delay systems. *Automatica* **2012**, *48*, 2159–2167. [CrossRef]
23. Altintas, G.; Aydin, Y. Optimization of Fractional and Integer Order PID Parameters using Big Bang Big Crunch and Genetic Algorithms for a MAGLEV System. *IFAC-PapersOnLine* **2017**, *50*, 4881–4886. [CrossRef]
24. Karahan, O. Design of optimal fractional order fuzzy PID controller based on cuckoo search algorithm for core power control in molten salt reactors. *Prog. Nucl. Energy* **2021**, *139*, 103868. [CrossRef]
25. Fu, W.; Wang, K.; Li, C.; Tan, J. Multi-step short-term wind speed forecasting approach based on multi-scale dominant ingredient chaotic analysis, improved hybrid GWO-SCA optimization and ELM. *Energy Convers. Manag.* **2019**, *187*, 356–377. [CrossRef]
26. Altbawi, S.M.A.; Mokhtar, A.S.B.; Jumani, T.A.; Khan, I.; Hamadneh, N.N.; Khan, A. Optimal design of Fractional order PID controller based Automatic voltage regulator system using gradient-based optimization algorithm. *J. King Saud Univ.—Eng. Sci.* **2021**, *in press*. [CrossRef]
27. Shouran, M.; Alsseid, A. Particle Swarm Optimization Algorithm-Tuned Fuzzy Cascade Fractional Order PI-Fractional Order PD for Frequency Regulation of Dual-Area Power System. *Processes* **2022**, *10*, 477. [CrossRef]
28. Rajesh, R. Optimal tuning of FOPID controller based on PSO algorithm with reference model for a single conical tank system. *SN Appl. Sci.* **2019**, *1*, 1–14. [CrossRef]
29. Bingul, Z.; Karahan, O. Comparison of PID and FOPID controllers tuned by PSO and ABC algorithms for unstable and integrating systems with time delay. *Optim. Control Appl. Methods* **2018**, *39*, 1431–1450. [CrossRef]
30. Osinski, C.; Silveira, A.L.R.; Stiegelmaier, C.; Bergamini, M.G.; Leandro, G.V. Control of ball and beam system using fuzzy PID controller. In Proceedings of the 2018 13th IEEE International Conference on Industry Applications (INDUSCON), Sao Paulo, Brazil, 12–14 November 2018; pp. 875–880. [CrossRef]
31. Šitum, Ž.; Trslić, P. Ball and beam balancing mechanism actuated with pneumatic artificial muscles. *J. Mech. Robot.* **2018**, *10*, 055001. [CrossRef]
32. Hannan, M.A.; Ghani, Z.A.; Hoque, M.M.; Ker, P.J.; Hussain, A.; Mohamed, A. Fuzzy logic inverter controller in photovoltaic applications: Issues and recommendations. *IEEE Access* **2019**, *7*, 24934–24955. [CrossRef]
33. El Ouanjli, N.; Motahhir, S.; Derouich, A.; El Ghzizal, A.; Chebabhi, A.; Taoussi, M. Improved DTC strategy of doubly fed induction motor using fuzzy logic controller. *Energy Rep.* **2019**, *5*, 271–279. [CrossRef]
34. Kennedy, J.; Eberhart, R. Particle Swarm Optimisation. In Proceedings of the ICNN'95—International Conference on Neural Networks, Perth, WA, Australia, 27 November–1 December 1995; pp. 1942–1948. [CrossRef]
35. Shi, Y.; Eberhart, R. A Modified Particle Swarm Optimizer. In Proceedings of the 1998 IEEE International Conference on Evolutionary Computation Proceedings, IEEE World Congress on Computational Intelligence (Cat. No.98TH8360), Anchorage, AK, USA, 4–9 May 1998; pp. 69–73. [CrossRef]
36. Solihin, M.I.; Tack, L.F.; Kean, M.L. Tuning of PID Controller Using Particle Swarm Optimization (PSO). *Int. J. Adv. Sci. Eng. Inf. Technol.* **2011**, *1*, 458. [CrossRef]
37. Mishra, A.K.; Das, S.R.; Ray, P.K.; Mallick, R.K.; Mohanty, A.; Mishra, D.K. PSO-GWO Optimized Fractional Order PID Based Hybrid Shunt Active Power Filter for Power Quality Improvements. *IEEE Access* **2020**, *8*, 74497–74512. [CrossRef]
38. Shouran, M.; Anayi, F.; Packianather, M.; Habil, M. Different Fuzzy Control Configurations Tuned by the Bees Algorithm for LFC of Two-Area Power System. *Energies* **2022**, *15*, 657. [CrossRef]